AD-A125 284 ON THE QUANTITATIVE ANALYSIS OF LIQUID FLOW IN PHYSIOLOGICAL TUBES(U) WISCONSIN UNIV-MADISON MATHEMATICS RESEARCH CENTER H WINET DEC 82 1/1

UNCLASSIFIED MRC-TSR-2456 DAAG29-80-C-0041 F/G 6/16 NL

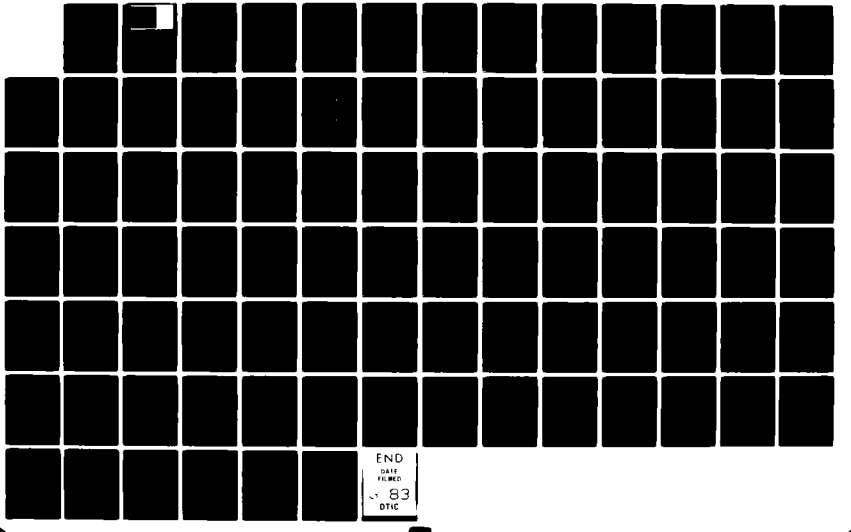

END
DATE FILMED
83
DTIC

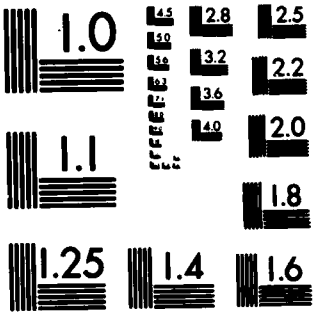

MRC Technical Summary Report #2456

ON THE QUANTITATIVE ANALYSIS OF LIQUID FLOW IN PHYSIOLOGICAL TUBES

H. Winet

Mathematics Research Center
University of Wisconsin—Madison
610 Walnut Street
Madison, Wisconsin 53706

December 1982

(Received October 8, 1982)

Sponsored by

U. S. Army Research Office
P. O. Box 12211
Research Triangle Park
North Carolina 27709

and

National Institutes of Health
Bethesda, Maryland 20205

UNIVERSITY OF WISCONSIN - MADISON
MATHEMATICS RESEARCH CENTER

ON THE QUANTITATIVE ANALYSIS OF LIQUID FLOW IN PHYSIOLOGICAL TUBES

H. Winet*

Technical Summary Report #2456

December 1982

ABSTRACT

We review three benchmark quantitative models for flow generation by physiological tube pumps. In each case significant differences between model predictions and tube behavior was emphasized. In order to close these gaps both modeler and Physiologist (often the same investigator) need to find paths which can grow to bridges. The modeler must develop more exact solutions to provide Physiologists with plug-in equations which will accept measurements. The Physiologist must make the kind of measurements which can be reasonably tested by a meaningful model. The measurements which have been featured in this review are pressure, viscosity and geometry--- where geometry varies with time, kinematic data. A number of diagnostic marker formulas have been presented as stepping stones to modeling. These include $\bar{R}_e$, $\bar{\beta}$, slenderness etc. which translate physiological data into indicators for modeling directions.

AMS (MOS) Subject Classification: 76Z05

Key Words: Flow in physiological tubes, pulsatile flow, ciliary flows, peristaltic/segmented flows, combination pumps.

Work Unit Number 2 - Physical Mathematics

*University of Southern California School of Medicine, University of Wisconsin Mathematics Research Center and California Institute of Technology Division of Engineering and Applied Science.

Sponsored by the United States Army under Contract No. DAAG29-80-C-0041. Supported in part by National Institutes of Health, Grant HD-51442.

TABLE OF CONTENTS

ON THE QUANTITATIVE ANALYSIS OF LIQUID FLOW IN PHYSIOLOGICAL TUBES

H. Winet*

I. INTRODUCTION: The Fluid Mechanical Approach to Tube Flow Modeling

Data gathered from measurements of contraction, pumping, viscosity, pressure and liquid flow in the various physiological tubes may be mapped onto numerous graphs without concern for their physical meaning. In addition to such empirical modeling these same data may be plugged into equations which represent models with a sound basis in Mechanics. This review presents these fundamental equations as plug-in forms which have been obtained by simplification of the fluid mechanical versions of Newton's laws of motion.

We also attempt to sketch how the plug-in forms are derived, what they mean and why they are or are not close to predicting our observations. The terminology is meant to be understood by physiologists with only sufficient training to know heuristically what mathematical integration is about. Here are some modeling definitions which we keep in mind and which will help orient the reader:

Empirical model A mathematical equation of the form $y = f(x,t)$ which represents an observed data relationship. Empirical models need have no physical meaning. e.g. Growth curve equations.

Experimental model A physical system which functions like another physical system sufficiently to give valid insight to the operations of the latter. e.g. squid axon.

Theoretical model A mathematical equation based upon the laws of Physics. In mechanics all theoretical models are developed from $F = ma$. They may be transformed at three levels into e-

* University of Southern California School of Medicine, University of Wisconsin Mathematics Research Center and California Institute of Technology Division of Engineering and Applied Science.

Sponsored by the United States Army under Contract No. DAAG29-80-C-0041. Supported in part by National Institutes of Health, Grant HD-51442.

quations which generate numbers.

Level 1-- ANALYTICAL SOLUTION/MODEL. An equation which results by solving F=ma without introducing any constants or parameters other than zero. The most general form of solution.

Level 2-- EXACT SOLUTION/MODEL. An equation which results by solving F=ma without introducing any constants or parameters other than those with delineated physical meaning.

Level 3-- NUMERICAL SOLUTION/MODEL. An equation which results by solving F=ma after introducing arbitrary constants or parameters which may have no physical meaning. In current application, a computer-intensive solution.

Why lump all body tubes together in one review when their physiological functions differ so greatly? Because fluid mechanically their function is the same; to transport liquids (and in some cases solids) and an understanding of how the pump(s) in any tube generate bulk flow gives us insight to the mechanics of other tube pumps. Such understanding develops from the construction of models from the fundamental equation of motion for all liquids. This fundamental equation is a form of Newton's Second Law (F=ma) the Navier-Stokes (N-S) equation which takes the mathematical form for an infinitesimal increment--call it a 'particle'--of fluid

$$dF = dF_g + dF_p + dF_v = \frac{dmv}{dt} \qquad (1)$$

where the symbol 'dF' (with or without subsscript) represents that amount of force acting on any particle of fluid and dmv/dt the change in velocity and mass with time of that particle as a result of the accelerations from all of the forces cited.

For physiological fluid flows the important forces are gravity F_g, that due to pressure F_p and that due to viscous drag F_v. The simple appearance of (1) is deceiving. When the right side is expanded to show the acceleration imposed by each force on a fluid particle, it is seen that even if we assume the particle mass remains constant, some 16 partial differential equation terms are required to account for three-dimensional effects. When the left side (the three ρF terms) is similarly expanded, over 30 partial differential terms appear because we have to account not only for three-dimensional effects but for the difference between forces and stresses (force/unit area) such as pressure and viscous drag as well. The quantitative theoretical model is spatially 'solved' when we add all these incremental effects together to describe the motion of a volume of fluid during an increment of time. This addition requires mathematical integration of (1) in all three dimensions. Unfortunately, no one has been able to perform such an integration and the only hope for obtaining a useful model which will predict flow in a given tube is to simplify the N-S equation sufficiently to make it solvable (able to be integrated).

Accordingly, Applied Mathematicians and Scientific Engineers who develop fluid mechanical models seek to convert as many of the partial differential terms into constants (or at least ordinary differentials) as possible. But the decision as to which terms may be simplified (i.e. "linearized") without loss of physiological significance must be made by biologically-oriented scientists who are familiar with the pumps and tubes of interest. It is the Physiologist who must supply the critical data by utilizing expe-

rimental techniques which do not themselves alter the essential flow characteristics. The interdisciplinary team approach which results from such cooperation provides the greatest potential for the development of realistic theoretical models for physiological tube flow dynamics. Thus, for an investment of the expertise needed to obtain valid data, the Physiologist earns models which can be used to predict fluid propulsion for given tube and pump motions.

The single most effective tool for simplifying the N-S equations is the Reynolds number (R_e) which is a dimensionless parameter comparing inertial stresses--characterized by mass, size and speed--with viscous stresses. It exists in two main forms, a translatory form obtained for fluid far from the direct influence of pump oscillations

$$R_{et} = \frac{\text{inertial stresses}}{\text{viscous stresses}} = \frac{\rho \bar{U} r}{\eta} \qquad (2)$$

and an oscillatory form obtained for fluid under the direct influence of pump oscillations

$$R_{ef} = \frac{\rho f r^2}{\eta} \qquad (3)$$

where ρ is fluid density (average density if m varies), $\bar{U}$ the average fluid velocity, r the tube radius, f the pump oscillation frequency, and η the fluid viscosity. The value of R_e does not have to be known precisely, as it is only a guide which indicates to the modeler which terms may be dropped from the N-S equation.

An example of its relationship to flow is presented in Table 1 which applies to flow in a rigid tube due to an unspecified pump.

Table 1

R_{et} Range	Type of Flow	Simplified form of N-S Equation
$R_{et} < 2100$	laminar	Stokes
$2100 < R_{et} < 4000$	unsteady (transitional)	Darcy-Weisbach
$4000 < R_{et}$	turbulent	Reynolds

II. The classification of Physiological tube flows

"Tube flows" is one class of "Internal flows" which is defined as any bulk flow within a container whose walls do not translate with the liquid. A tube is a container open at each end which is longer than wide, generally speaking, by a slenderness ratio $L/2r$ of at least $0.03\ R_{et}$ for laminar flow (see below) and $0.7R_{et}^{0.25}$ for turbulent flow (Caro et al, 1978).

We distinguish three classes of tube flows according to their pumps as diagrammed in Figure 1. The two most noteworthy features in each diagram are the direction of the pressure gradient (Is pressure higher upstream or downstream?) and the curvature of the flow velocity profile (the dashed line which is a plot of fluid particle velocity as a function of distance from the endothelium). The simplest flow shown is pulsatile flow which is generated by an upstream valved pump, the heart, and characterized by an upstream pressure which is higher than the downstream pressure and a flow velocity profile with no reflux (syn.: retropulsion). The

Pumping in Biological Tubes

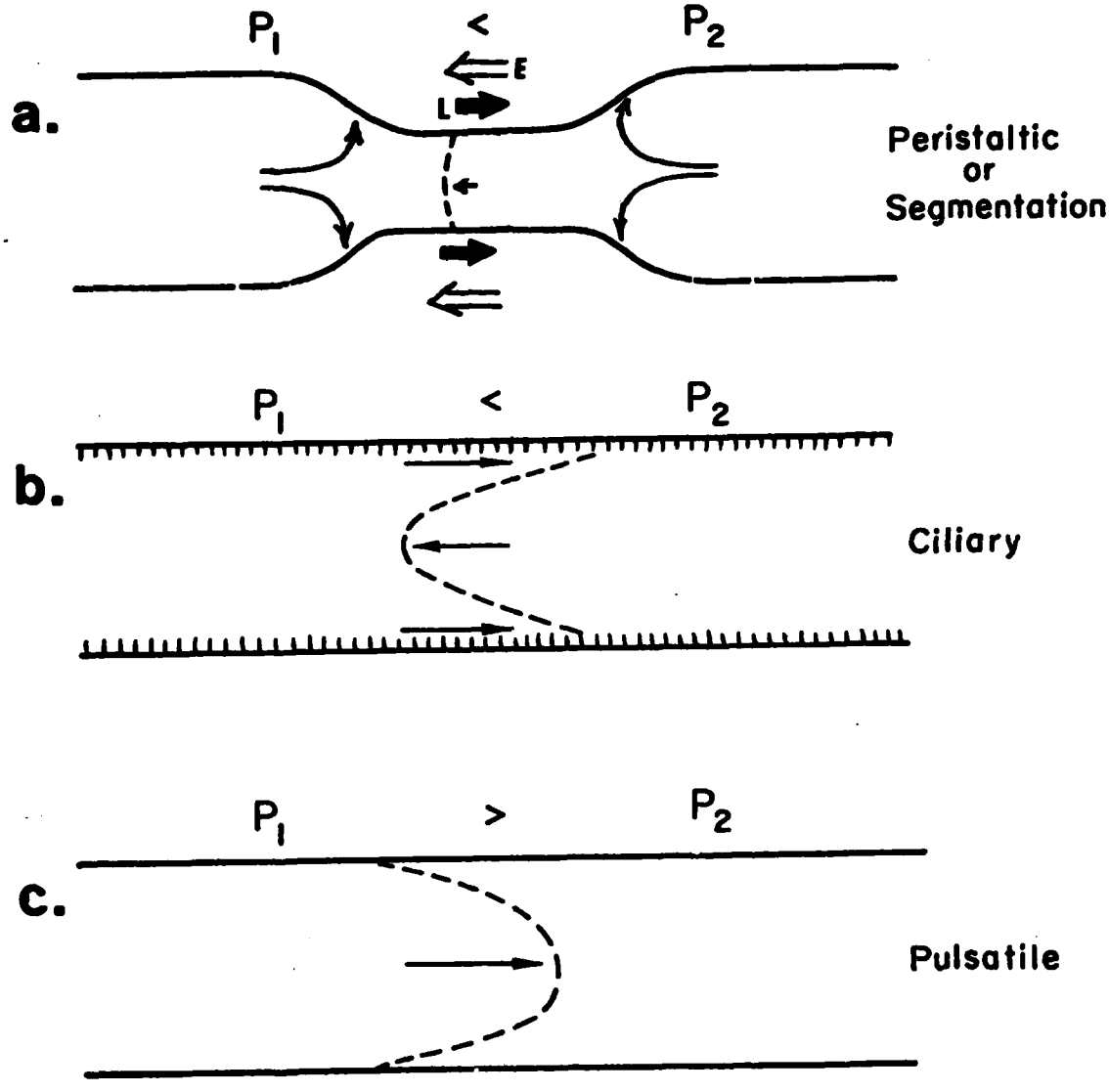

FIGURE 1.

Three classes of physiological tube propulsion. a. Peristaltic/ Segmental or Propagativ/Stationary constriction pumping includes active deformation of tube walls and considerable lumen occlusion. Flow velocity profiles show substantial reflux and downstream pressure P_2 always exceeds upstream pressure P_1. b. Ciliary pumping is developed by arrays of oscillating slender bodies attached to the lumen wall. Fluid particle speeds are highest near the ciliary tips and flow velocity profiles show reflux as a rule because $P_2 \not> P_1$. c. Pulsatile flow is generated by an upstream valved pump which creates a $P_1 \not> P_2$. The resulting flow velocity profile rarely shows reflux where flow is steady and the walls contribut to propulsion primarily passively, i.e. through their elastic properties. L_s = sublayer thickness.

next simplest is ciliary flow which is generated by an array of pumps lining the endothelium and characterized by an upstream pressure which is lower than the downstream pressure and a flow velocity profile showing reflux. The most complex flows are the peristaltic/segmental types (syn.: propagative/stationary constrictions (Macagno and Christensen, 1980)) which are generated by tube constrictions which may (peristaltic) or may not (segmental) be propagated. Peristaltic flows are characterized by an upstream pressure which is lower than the downstream pressure and a flow velocity profile showing reflux. It should be noted that these flow profiles are idealized in order to be instructive; so it is not surprising to an experienced modeler that when a peristaltic wave passing over the antrum of the stomach encounters a wide open pylorus, the flow velocity profile of the chyme will show virtually no reflux.

The distribution of these flows according to the organs to which they contribute and the contractile tissue of the pump are summarized in Table 2. We have omitted cytoplasmic flows (such as occurs in axons) and filtration because the former has the unusual added quality of being at least partly generated by the fluid itself and the latter is an extension of pulsatile flow although as we shall show it interacts with other pumps in what we call "combination pumps".

Table 2

System	Pump Contractile Tissue: Cardiac Muscle	Ciliated Epithelium	Skeletal Muscle	Smooth Muscle
CNS(Ventricles)	-	C	-	-
Circulatory*				
Heart	Pu/P(?)	-	-	-
Macrocirculation, Precapillary	Pu	-	-	+
Microcirculation	Pu	-	-	Sph.
Macrocirculation, Postcapillary	Pu	-	Squeeze	-
Digestive				
Esophagus	-	-	-	P
Stomach	-	-	-	P
Small Bowel	-	-	-	S/P
Large Bowel	-	-	Sph.	S/P
Excretory	-	-	Sph.	P
Lungs(non-mucus unless plugs)	-	C	-	-
Reproductive				
Cervix	-	C	-	S/P(?)
Uterus	-	C	-	S/P
Oviduct	-	C	-	S/P(?)
Efferent Ducts	-	C	-	S/P(?)
Epididymis	-	-	-	S/P(?)
Vas Deferens	-	-	-	S/P(?)

*Flow in any blood vessels feeding muscle is affected by contraction of the muscle. C = Ciliary, P = Peristaltic, Pu = Pulsatile, S = Segmental, Sph. = in sphincters, + = Propulsive effect through 'elastic' recoil

Upon considering the widespread occurence of contractile tissue and the features emphasized in Figure 1 and Table 2, one is struck by the variety of forms these tissues have assumed to make liquids flow and the variety of mechanisms employed to create a pressure gradient which will maintain this flow.

III. The Poiseuille (Hagenbach) equation as a reference model for all physiological flows.

In 1841 J.L. Poiseuille, a physician with a talent for per-

forming experiments, published an empirical equation for volumetric flow rate (Q) in a cylindrical tube as a function of pressure head and tube diameter. The equation contained no explicit terms for viscous forces. But in spite of this omission and the fact that it was not until 1860 that E. Hagenbach (and, independently, F. Neuman) obtained a theoretical form of the model, it is the theoretical equation which today bears Poiseuille's name (Rouse and Ince, 1957)

$$Q = \frac{\pi r^4 \nabla P}{8\eta} \qquad (4)$$

where ∇P, often written $\Delta P/L$ is the pressure gradient along the tube axis. The Hagenbach model was obtained by direct integration of the N-S equation after first making the following simplifications (fluid mechanics synonyms in parentheses):

1. R_{et} is small enough so that the fluid is stable.
2. density ρ is constant (incompressibility).
3. The flow pattern does not change with time (steadiness)
4. viscosity η is constant (Newtonian flow). Non-Newtonian flow means that the rate of flow (strain) is not linearly proportional to the amount of shear (stress) applied. Viscosity is the slope of the curve relating fluid strain to stress.
5. The flow pattern does not change with position along the tube axis (negligible entrance or exit effects).
6. Fluid particles are so close to one another that they are not distinguishable as individual (continuity).
7. The fluid particles touching the tube wall are stuck to it (the no-slip boundary condition).
8. The tube walls do not deform (the rigid boundary condition).
9. Gravitational influences are negligible.

The experienced Physiologist can call to mind violations of each of these basic assumptions while at the same time marveling at how

well the Poiseuille model has predicted flow in many circulatory tubes. The simplified form of the N-S equation resulting from these assumptions has only 9 partial differential terms on the right side and 12 (non-linear and second order) on the left and is known as the Stokes equation. At the time of Hagenbach this equation was still not integrable so he added the final assumption that

> 10. all translating fluid particles moved in the same direction (laminar flow).

He then obtained the "one-dimensional" Stokes equation for a tube

$$\frac{dP}{dx} = \frac{\eta}{r}\frac{d}{dr}\left(r\frac{dU}{dr}\right) \qquad (5)$$

an ordinary differential equation (of second order) with U the fluid particle velocity in the axial direction x which is the only flow dimension.

One can imagine dP/dx becoming ∇P, dU becoming Q and dr filling in the essential contributions of tube geometry ($\pi r^4/8$) upon complete integration of (5). The most critical tests for tube flow models do not, however, require complete integration of the equation of motion. If flow is laminar, integration in one dimension gives the equation for the flow velocity profile:

$$U(r_i) = \frac{\nabla P(r_i^2 - r^2)}{4\eta} \qquad (6)$$

where r_i is any distance from the tube axis. Flow velocity profiles are more discriminating tests of model validity because they

give a more detailed picture of the flow pattern than the single value Q. A comparison of measured with theoretical flow velocity profiles, accordingly, is commonly the best test of a model.

The theoretical models for ciliary and peristaltic flows have to develop along similar paths because the rules of physical analysis are quite strict. The fact that their pumps reside in the tube wall leads us to expect that their flow velocity profiles are more complicated and they are. But the basic model structure persists:

VELOCITY IS DIRECTLY PROPORTIONAL TO PRESSURE GRADIENT AND TUBE CALIBER AND INVERSELY PROPORTIONAL TO VISCOSITY

or $$U(r_i) = K \nabla P \, f(r_i)/\eta$$

where $f(r_i)$ is some geometric function and K a proportionality constant.

This pattern is readily evident in the Blake (1973) model for ciliary flow:

$$U(r_i) = U_m - \frac{\nabla P \, (r^2 - r_i^2)}{2\eta} \qquad (7)$$

where U_m is the maximum fluid particle velocity, and it is discernable after careful examination of the Shen (1976) model for peristaltic flow:

$$\bar{U}_T(0) = c_p \left[\frac{\Delta P_T R_e}{\rho \, c_p^2} \left(1 - \frac{M_1}{M_2}\right) + 2\left(1 - \frac{M_1^2}{M_2}\right) \right] \qquad (8)$$

where $\bar{U}_T(0)$ = average fluid velocity along the axis (0) over one wave period T

ΔP_T = average pressure change over one period

c_p = peristaltic wave velocity

$M_1 = 1/(1 - \phi^2)^{1.5}$

$M_2 = (1 + 1.5\phi^2)/(1 - \phi^2)^{3.5}$ with $\phi = 1 - a/2r$ the occlusion ratio

and a = tube caliber at the constriction.

The viscosity term is hidden, of course, in the R_e denominator. In this equation the need for profile restriction to the axis and velocity averaging is dictated by the changing flow directions during each wave cycle.

The in vivo mechanical conditions of most physiological tube flows seem a far cry from the flows represented by these three models. Yet each can claim some predictive success in spite of its simplicity. To be sure, more complex models will be necessary for more accurate predictions of flow in such vessels as the heart, stomach and brain ependyma, but they will not result from a return to the full N-S equation and application of it directly to the tube in question. Rather, they will result from step-by-step complication of the simple models without losing the umbilicus to physical reality--the rules of physical analysis. The direction of these complications must be determined by a pooling of the expertise of Physiologists and Fluid Mechanicists. The former will indicate which part of the model must be improved and the latter will perform the improvements made possible by the latest advances in Applied Mathematics.

In the following sections we shall summarize the success of

the three quantitative theoretical tube flow models by comparing predicted with measured flow velocity profiles where possible. For those instances where significant disagreement exists we shall attempt to indicate where the model must be complicated to improve its accuracy. As the reader may anticipate, the improvements will be directed toward the form of ∇P, η or $f(r_i)$.

IV. Pulsatile Flow

The field of cardiovascular fluid dynamics was active before the work of Poiseuille and the amount of data gathered to date is impressive (see for example Caro et al, 1978). Yet flow velocity profiles *in vivo* have been obtained only within the last 20 years (Bergel and Schultz, 1971) and these have been limited to the aorta. Nevertheless, the data so far accumulated provide ample bases for pinpointing specific model needs.

The circulatory system may be divided into four fluid dynamical sections in terms of the relative affect of pressure, viscosity and geometry on flow in each:

1. Heart flow-- Two parallel pumps
    a. venous-to-pulmonary segment
    b. pulmonary-to-aorta segment
2. Aorta-arterial flow-- Output macrocirculation
3. Arteriolar-capillary-venular flow-- Microcirculation
4. Venous flow-- Input macrocirculation

A. Heart flow

The heart may be thought of as two check valve pumps in parallel as indicated in Figure 2. While the two pumps are in fact in contact and not strictly mechanically independent, they are sufficiently separated by microcirculation to be modeled indepen-

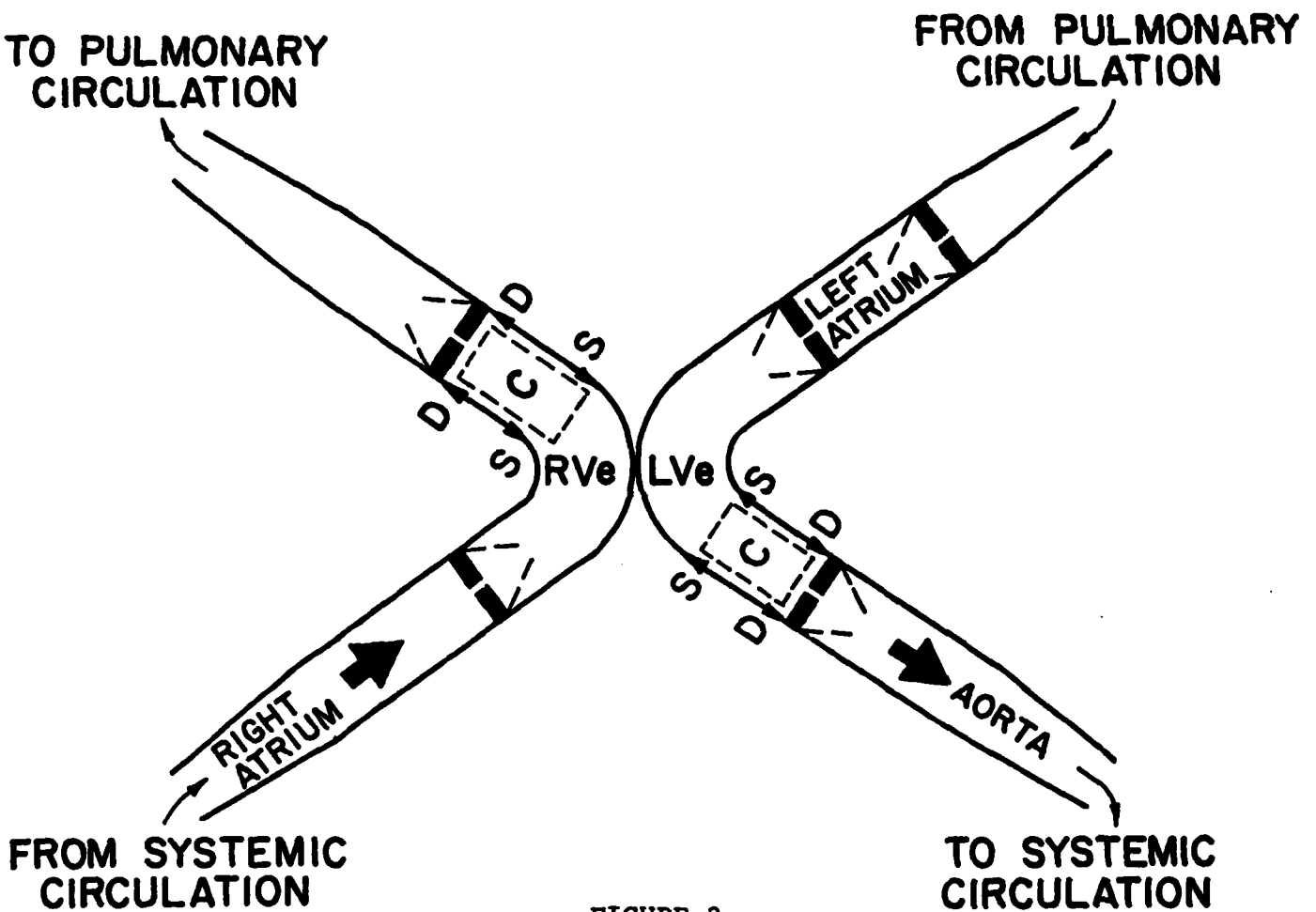

FIGURE 2

The heart modeled as two parallel curved check valve pumps. Given a constant volume C, the pump walls operate as if they slide over C; at systole S (see arrows) in the upstream direction forcing the valves to open (to the dashed line positions) and at diastole D (see arrows) in the downstream direction while the valves close. The function of the pumps is to raise the pressure from the 'dissipated' level at which it enters the atria to a sufficient head to push the blood through the pulmonary/systemic tube networks.

dently. The first, a two-valve pump propels blood into the pulmonary circulation at a pressure which oscillates between 1.17×10^3 and 3.12×10^3 N m^{-2}. The second, a three-valve pump propels blood into the systemic circulation at a pressure which oscillates between 1.04×10^4 and 1.56×10^4 N m^{-2}. The movements of the ventricular walls suggest peristalsis-like waves and a recent careful analysis of these movements by Klausner et al (1982) lends weight to this suggestion. Atrial contractions, however, are much less wavelike. The heart pumps are the only components of the circulatory system in which the downstream pressure is higher than the upstream pressure. It is of course the pressure-generating energy of cardiac muscle that is dissipated by viscous stresses to yield the pressure gradient of blood flow.

Since the tube walls of the heart do deform, assumption number 8 for the development of the Poiseuille model is violated. Moreover, the speed of blood flow varies at different points in the heart but can exceed 100cm/sec and give Reynolds numbers (see Table 3) for which we would expect non-laminar flow (see Table 1). There is turbulence in the heart but mainly around the valves where vortex flow (a doughnut of fluid which flows through the doughnut hole and around the outer rim) has been observed. Its prediction, however, appears to be more dependable if the non-dimensional parameter

$$S_r = \frac{L_v}{U_m T} = \frac{f L_v}{U_m} \qquad (9)$$

the Strouhal number(= 'reduced frequency') is used (Lee and Talbot, 1979) because laminar flow has been observed near the aortic

PUMP / Tube	c Propagated wave velocity -cm/sec-	pump beat or constriction frequency -Hz-	L/2r tube slenderness -	Q volumetric flow rate -cc/sec-	2r average caliber -cm-	U_m maximum or bolus velocity -cm/sec-	$\dot{\gamma}$ wall shear -1/sec-or λ propagated wave length -cm-	ϕ occlusion ratio -	VP pressure gradient mm Hg/cm	R_{et} Reynolds Number -	η fluid viscosity -cp-	R_{ef} unsteady -
PULSATILE.....Pressure waves							$\dot{\gamma}$					α
Heart	-	1.1	$\angle 6^t$	107	$\angle 2x5^t$	71000^d	-	$\angle 1$	-	$\nearrow 4500^d$	3^g	$\nearrow 20^d$
Ascending Ao.	500^d	1.1	3.3^d	60^d	1.5^d	290^d	107^*	$\angle 0.1$	0	4500^d	3^g	13.2^d
Descending Ao.	500^d	1.1	15.0^d	13-53*	1.3^d	250^d	123^*	$\angle 0.1$	0	3400^d	3^g	11.5^d
Femoral Art.	900^d	1.1	25.0^d	1.3-1.9*	0.4^d	120^d	200^*	$\angle 0.1$	-	1000^d	3^g	3.5^d
Arteriole	-	1.1	30.0^d	$(4-8)x10^{-5*}$	0.005^d	1.0^d	1200^*	$\angle 1$	$0.74-1.47^d$	0.09^d	2.3^g	0.04^c
Capillary	-	1.1	1000^d	$(2-20)x10^{-8*}$	0.0006^d	0.17^d	933^*	$\angle 0.1$	$4.41-8.82^d$	0.001^d	2.0^g	0.005^a
Venule	-	1.1	37.5^d	$2x10^{-5d}$	0.004^d	0.5^d	700^*	$\angle 0.1$	-	0.035^d	2.3^g	0.035^d
Inf. Vena Cava	400^d	1.1	30^d	25^d	1.0^d	25^d	150^*	$\angle 0.3$	-	700^d	3^g	8.8^a
CILIARY.....Metachronal wave							$\dot{\gamma}$					R_{ef}
Stem Embryo	-	21.0^m	4.0^m	-	0.01^m	0.07^m	-	$\angle 0.1$	-	$\angle 0.01$	-	$\angle 0.01$
Effnt Ducts	-	-	500.0^b	$3.3x10^{-8b}$	0.005^b	-	-	-	-	$\angle 0.01$	10^g	$\angle 0.01$
Ovid. Isthmus	-	20.0^b	130.0^b	-	0.05^b	-	56^r	-	-	$\angle 0.01$	-	$\angle 0.01$
PERISTALTIC....Constriction waves							λ_p					
Esophagus	4^n	-	$\angle 9^n$	-	$\angle 2^n$	4^n	-	$\angle 1.0$	-	$\nearrow 1$	-	$\nearrow 1$
Duodenum	$4-10^h$	-	11.6^h	10.5^h	3.8^h	-	-	-	20^{**}	$\nearrow 1$	-	$\nearrow 1$
Jejunum	-	-	-	-	-	-	-	-	-	$\nearrow 1$	-	$\nearrow 1$
Ileum	-	-	129	-	2.4	-	-	-	20.3^{**}	$\nearrow 1$	-	$\nearrow 1$
Colon	2.5^e	-	37.5^e	5^f	4.0^e	0.083^f	21^f	-	50^{**q}	$\nearrow 1$	-	$\nearrow 1$
Ureter	3^a	0.062^k	155	$2.8x10^{-3a}$	0.2	3^a	7.5^a	$\swarrow 0.96$	15^{**q}	$\angle 1$	0.7	-
SEGMENTATION...Migrating patterns												
Duodenum	$0.08-0.133^h$	0.197^f	-	-	3.8^h	-	45^p	-	20^{**f}	$\nearrow 1$	-	$\nearrow 1$
Jejunum	-	-	-	0.008^j	-	0.21^c	-	-	15^{**c}	$\nearrow 1$	-	$\nearrow 1$
Ileum	$0.017-0.033^h$	0.156^f	-	0.021^j	2.4	-	4.6^p	-	-	$\nearrow 1$	-	$\nearrow 1$

PHYSIOLOGICAL TUBE FLOW VARIABLES

* calculated, ** point pressure, a= Boyarsky & Weinberg (1973), b= Brennen & Winet (1977), c= Bueno et al (1975), d= Caro et al (1978), e= Christensen (1981), f= Davenport (1977), g= Fung (1981), h= Grivel & Ruckebusch (1972), j= Kerlin et al (1982), k= Melchior & Lutseyer (1973), m= Nelson & Wright (1974), n= Vantrappen & Hellemans (1980), p= Weems (1981), q= Weinbrodt (198 1), r= estimated from Winet (1976), s= Winet (1980), t= Yang et al (1978).

Table 3

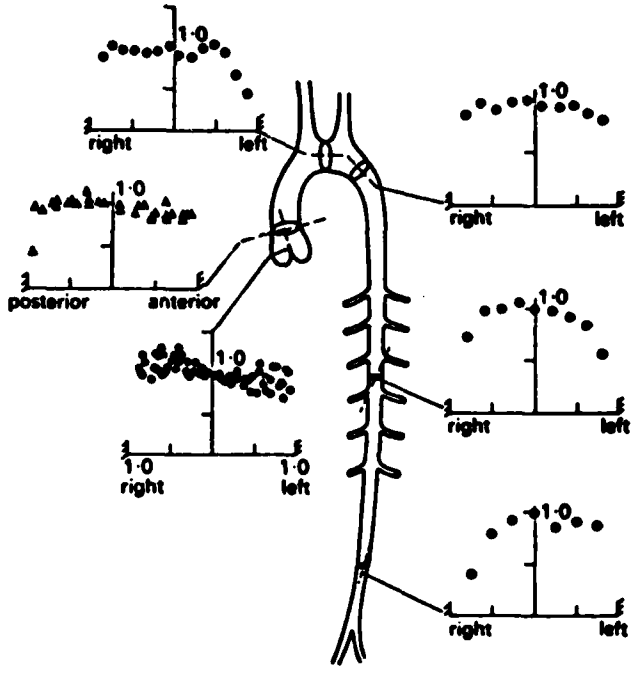

FIGURE 3

Net flow velocity profiles along the aorta as measured by Schultz et al (1949). Each graph shows the profile of mean velocities relative to the center-line mean velocity.

valve at R_e values above 4300 (Schultz et al, 1969) and S_r is a more direct measure of unsteadiness. Here U_m is axial velocity of the blood, L_v is valve length and T is cardiac cycle period. If $S_r < 0.01$ quasi-steadiness may be assumed. If $S_r > 0.01$, flow is unsteady and regurgitation (turbulence) may appear at relatively small values of R_e. There are also geometric violations of the simplifying conditions. Given its R_e, it is difficult to call even the longest chamber of the heart, the left ventricle, a tube because its slenderness ratio of about 6 (11.5cm/2cm) is just barely that required ($0.7 \times 4500^{0.25}$ = about 6) to escape entrance/exit effects and when its flow gives a R_e = 8000 it is too short. Thus we have violations of conditions 1, 3, 5, 8 and 10 in the pump and cannot reasonably expect the Stokes equation or the Poiseuille model to apply.

B. Output macrocirculation

1. Pressure effects

Net flow velocity profiles along the aorta show an increasing tendency toward the quadratic form predicted by the Poiseuille equation with distance from the aortic valve as shown in Figure 3. It will be noted that each profile is an average because the pressure wave will enhance or reduce instantaneous particle translation at a point depending on which part of the wave is passing. The relationship between the pressure waves and net particle motion must, consequently, be accomodated in any accurate model.

a. The Womersley parameter

When blood exits the aortic valve its R_e is above 4500 and is turbulent but the turbulence does not spread beyond the imme-

diate vicinity of the aortic valve unless

(a) the aortic walls are abnormally rough
(b) the lumen is abnormally narrowed (stenosis)
(c) there are projections into the lumen
(d) red blood cells are abnormally rigid
(e) hematocrit is abnormally low

However, R_{et} ignores the pulsatile nature of blood flow and thus must be replaced by a form of R_{ef}. The one used in cardiovascular analysis is the Womersley parameter

$$\alpha = r\sqrt{\frac{f\rho}{\eta}}. \qquad (10)$$

If $\alpha < 1$ then Poiseuille flow exists. If $\alpha > 4$ then an unsteady or oscillatory component must be included in the model for flow.

b. The propagating pressure wave

The physical source of the oscillatory component is the heart which sends out a pressure wave at an f = 1.1 Hz. If the blood vessel were rigid this wave would be transmitted immediately through the incompressible blood. The existence of a travelling pulse wave, therefore, is evidence of a flexible tube and when a pressure pulse reaches a given axial position x_i, r will increase. The speed of this increase and the recoil following passage of the pulse have a profound influence on the flow velocity profile at x_i. As r is increasing U_{xi} (axial flow at x_i) decreases because fluid is moving radially (U_r) i.e. toward the wall. Conversely, as r decreases U_{xi} increases because the trailing end of the recoil wave is increasing upstream P. The calculation of the changes in U_{xi} over one pulse cycle ($U_{xi}(t)$) would be relatively easy and if plotted would follow a wave form similar to but out of phase with the pulse wave by a constant amount <u>if</u> the vessel

were purely elastic. Moreover, when small amplitude waves are imposed artificially on an arterial segment, as they travel downstream their amplitude decreases much faster than in a purely elastic tube (Caro et al, 1978). A purely elastic solid obeys Hooke's law (Stress = E x Strain) where E is the elastic coefficient or Young's modulus. This equation has the same form as Newton's law for fluids (where η replaces E). Combining Hooke's law with the zeroth law of Laplace--P = $\tau\Delta w/r$--where Δw is the wall thickness and τ is tension, and following its change with time gives a measure of pulse wave velocity

$$c_o = \sqrt{\frac{E\Delta w}{2\rho r}} \qquad (11)$$

known as the Moens-Korteweg equation (although it was derived originally by T. Young in 1808).

Blood vessels are, of course, non-Hookean solids as E is not constant during the stretch-relax cycle response to a passing pulse. Given the composition of the blood vessel wall as smooth muscle with elastin and collagen fibers, its non-Hookean behavior is not surprising. Accordingly, the predicted phase difference between maximum pressure and maximum velocity at x_i is not confirmed and the construction of a model predicting $\bar{U}(r_i)$ at x_i which relates c_o to the equation of motion is now extremely difficult. Nevertheless, numerical solutions for volumetric flow rates have been developed assuming that the blood vessel is elastic but leaky and tapered (Guier, 1980) or that it is impermeable but not tapered (Gerrard, 1982).

2. Geometric effects

a. taper (cf. Walburn and Stein, 1981)

The inclusion of tapering in the Guier model is necessary because the aorta caliber tapers from 1.5 cm in the ascending aorta to 0.9 cm in the abdominal aorta and R_e does not include a taper factor. Taper places a greater pressure stress on the wall and helps create a higher pressure maximum in the pulse wave.

b. branching (cf. Walburn and Stein, 1980)

A more significant contributor to pulse wave amplification, however, is the branching of blood vessels into daughter vessels wherein flow dividers reflect pressure waves back into the oncoming waves. Each daughter tube is a new entrance at the flow divider where a blunt plug-like flow velocity profile is formed which must travel 0.03 R_e before it can fully develop a parabolic profile again. Secondary flows--fluid movements not parallel with the tube axis (e.g. vortex flow)--will develop at branchings if

$\beta \geq 1.2$ where

$$\beta = \frac{\sum A_i}{A_m} \qquad (12)$$

with A_i and A_m the cross-sectional area of each daughter branch and the mother branch respectively (Caro, 1978). In addition, a flow divider angle of more than 70° is likely to produce secondary flow.

c. curvature

When fluid is forced to follow a bend in a tube the fluid particles near the outer curvature must travel farther than those near the inner curvature to keep up with them. Since this acceleration requires an additional force and none exists, the flow ve-

locity profile axis drifts outward. The smaller the tube radius of curvature R_c, the greater the drifting tendency as indicated by the non-dimensional parameter, the Dean number.

$$D_u = R_e \left(\frac{r}{R_c}\right)^{0.5} \quad \text{(Ward-Smith, 1980)} \quad (13)$$

If $r/R_c < 10^{-2}$, R_e is sufficient to describe the flow regime (laminar, turbulent, etc.) but at all D_u values above 10^{-2} some secondary flow such as that shown in Figure 4 is predicted.

3. Viscous effects

At shear rates below 100 sec^{-1} whole blood is markedly non-Newtonian for normal hematocrits. In the microcirculation this effect is significantly altered by the small vessel caliber but in the macrocirculation the wall shear values, as shown in Table 3 insure Newtonian rheology near the wall. There is, however, an inertial effect by which the RBC's tend to gather near the tube axis. This tendency is called "tubular pinch" or the "Segre'-Silberberg effect. Its influence on flow in the macrocirculation is unknown. One may speculate, nevertheless, that while the 'free plasma' layer near the wall has an inherently Newtonian rheology, the central core of RBC's which is at a high hematocrit and experiences lower shear may well exhibit non-Newtonian behavior which could alter flow at tube bends and branches.

C. Microcirculation

Moving whole blood is classified in fluid mechanics as "multi-phase flow". Usually only plasma and RBC's are considered in any rheological evaluation of blood so it is often analysed as a two-phase flow system. As noted above, blood rheological properties

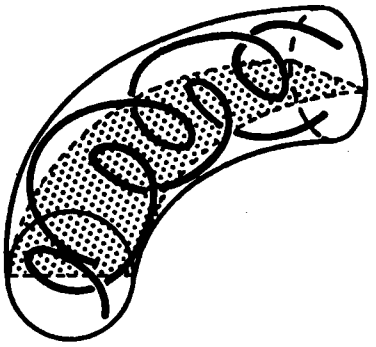

FIGURE 4

Secondary flow created by tube bending. Adapted from Talbot and Berger (1974).

have been relatively ignored in fluid mechanical analyses of the macrocirculation. One reason is the good agreement of flow velocity profiles with the Poiseuille model predictions--with some averaging of the pressure pulse effects--by the time the blood reaches the abdominal aorta.

But in vessels of less than 300μm caliber, 8μm wide dispersed phase particles with a volume fraction (hematocrit/100) of 0.48 can no longer be approximated as points in the fluid. Thus, while pressure effects dominate macrocirculation modeling, viscous effects dominate microcirculation modeling; due in part to RBC-RBC interaction and in part to RBC interaction with the tube wall where its caliber is small enough to inhibit the Segre'-Silberberg effect.

1. Viscous effects

a. bulk viscosity

In a two-phase flow system the viscosity of the total system or bulk viscosity is the result of the interaction of the dispersed phase particles with

(1) each other

(2) the continuous phase (e.g. plasma) and

(3) the wall.

Applied mathematicians analyzing multiphase flow are presently trying to model each of these interactions but have not developed anything useful to Physiologists beyond small improvements in the Einstein equation for viscosity of suspensions such as that of Batchelor (1974)

$$\eta = \eta_o(1 + 2.5h + 7.6h^2) \qquad (14)$$

where η_o is the continuous phase viscosity and h the volume fraction. The dispersed phase modeled by this equation is an array of hard spheres.

Interaction with the wall increases where RBCs moves into vessels of decreasing caliber. No physiologically applicable model exists for this flow system, however, until the tube caliber reaches 8μm or less. Then the wall shear, although quite high as indicated in Table 3, is less than in the arterioles. The main reason for the lower value of capillary wall shear is the non-rigidity of the RBC's and the effect of lubrication which is discussed under 'lubrication' below.

b. Fahreus-Lindqvist effect

Bulk viscosity of blood decreases in vessels of 300μm caliber or less from 0.03p to about 0.02p with decrease in r. These measurements were obtained by applying the Poiseuille model to observations of RBC velocities in vitro at known ∇P and r values. It is believed this Fahreus-Lindqvist effect is due primarily to the Fahreus effect (Skalak and Chien, 1981) wherein the hematocrit falls in the smaller blood vessels from its value in the output macrocirclulation (allowing the influence of the continuous phase to increase) and returns to its original value upon entering the input macrocirculation (venous system).

c. plasma skimming

A more dramatic viscosity difference develops in situ where a vessel branches and almost pure plasma drains into the smaller branch. As a result a dramatic decrease in viscosity takes place in the small vessel while an increase takes place in the larger

branch which has experienced a jump in hematocrit.

2. Geometric effects

a. branching

Progress in the development of flow models for the microcirculation has been slow not only because of the two-phase flow complication but because there is so much branching in microvascular beds that it has been difficult to detect the source and/or destination of flow viewed in a given segment. The beds are, of course, three-dimensional and one may conclude that an observed flow in one segment is due entirely to an observed tributary without being aware that there are tributaries above and/or below the plane of view.

b. physiological control

Precapillaries and precapillary sphincters which are indicated in Figure 5 interact via a feedback mechanism which is subject to local metabolic control. The control process is outside the limits of this review but the results, narrowing or closing off of branches, change r and create shifts in the microcirculation pattern. Thus, flow could be altered in any vessel under observation without the observer noting any geometric change in the bed within the field of view.

c. change in shape of RBC's

RBC's some 8μm in diameter can flow through capillaries with calibers as small as 2.8μm. The collagen/elastin ratio in capillary endothelium is high enough to keep these smallest capillaries from expanding any measureable amount to accomodate the RBC's they transport. Consequently, the geometry of the RBC must change al-

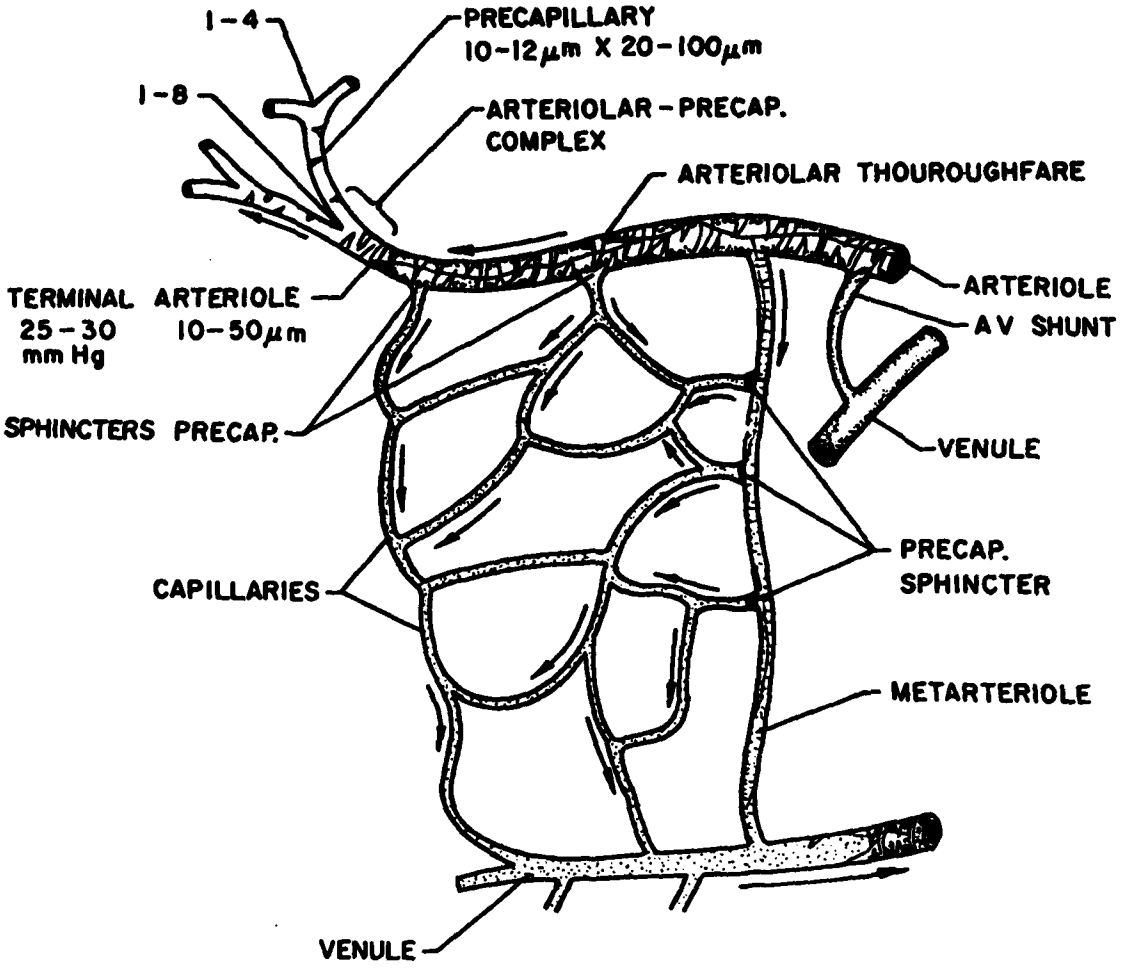

FIGURE 5

Microcirculatory bed adapted from Charm and Kurland (1974). Blood pathways are not preset and choices depend upon local conditions, particularly those which determine the contractile state of precapillary tubes, precapillary sphincters and metarterioles.

though the precise shape assumed is in some dispute (Bagge et al, 1980).

3. Pressure effects

a. pressure waves

Micropressure measuring devices such as those employed by Lipowsky and Zweifach (1977) have detected pressure pulse waves in the microcirculation. The rigidity of the microvasculature as expressed in the uniformity of the pulse waves, however, precludes any strong influence of wall deformation on net flow velocity profiles such as occurs in the aorta.

b. lubrication

When an RBC squeezes into a capillary less than 8μm in caliber it distorts but does not actually touch the wall because the fluid covering the wall (the no-slip layer) becomes a lubrication layer with a large radial fluid pressure which maintains a so-called lubrication gap of thickness b. As the RBC moves forward fluid must move back in the lubrication layer to conserve fluid mass. The interaction between the leak-back in the lubrication layer Q_b, the local pressure drop ∇P_b across the layer resulting from the piston-like movement U of the tight-fitting RBC and the geometry of the layer is modeled by lubrication theory with K a dimensional constant as

$$Q_b = \frac{b^3 \nabla P_b}{12\eta_o} + \frac{KbU}{2} \qquad (15)$$

which has an interesting resemblence to the Blake model for ciliary flow as may be perceived by examining (7) and will be more evident in the ciliary flows section. The leakback described by this equa-

tion fills in the space vacated by the translating RBC in a flow pattern termed "bolus flow". The interaction of bolus flow with the trailing RBC is a critical factor in determining U. That is, there is some separation distance for capillary RBC's at which U is optimal. The value of U here, in any case, is smaller than any U_o calculated from the Poiseuille model because the model 'fluid' is now an RBC. Consequently, wall shear appears smaller in capillaries than in arterioles as shown in Table 3.

4. Solid mechanical effects

In order to complete the model for movement of RBC's through the microcirculation, terms accounting for the solid mechanics or elastic properties of this non-Hookean cell must be derived. Such derivation is an active area of modeling at present (Skalak and Chien, 1981). One can see a parallel between the need for a non-Hookean model for arterial walls and one for RBC's in order to develop the complete flow model for each vessel.

D. Input macrocirculation

The flow patterns in the venous system deviate from the Poiseuille model primarily because

(1) Skeletal muscle contractions are requred to maintain flow and they are not in phase with heart pressure pulse waves

(2) Valves in veins prevent backflow except near the closure points and they are not in phase with heart pressure waves

(3) Veins are more collapsable than arteries and will change shape in response to their lower internal pressures

The dominant flow limiting quantity in the heart and output macrocirculation is pressure which is represented in (11). In the

microcirculation it is viscosity as represented in (14). In the input macrocirculation, geometry is the dominant modeling feature. This is not to belittle geometry in the rest of the circulatory system. After all, Q varies as r^4 while the other quantities are first degree. But the diagnostic flow velocity profile varies only as r^2 and geometric changes are less dramatic in the prevenous systemic circulation.

1. Geometric effects

a. confluence

Where venules join to form veins and veins join to form vena cavae there is an entrance effect of meeting streams. Since the axes of the net flow velocity profiles of the joining streams are at first not in the center of the main tube, the mainstream profile will look like a '3', gradually flattening out and eventually forming a single parabola. Laminar flow is expected, given the relatively low R_e and the slenderness of the tubes (see Table 3). The minimum slenderness ratio required for flow development in, for example, the inferior vena cava is 0.03x700 = 21 which is less than the slenderness value shown in the table.

b. collapsability

In general veins have thinner walls (Δw is less), less elastin and more collagen than arteries of equal caliber. Consequently they tend to be more flaccid. Where venous lumen pressure P_L is greater than or equal to interstitial hydrostatic pressure P_I the vessel retains its circular shape. But in the anterior venous branches of the upright individual and all veins being squeezed by skeletal muscle or the abdominal-thoracic pump, $P_L \angle P_I$ and the vessel 'collapses' into an elliptical-to-dumbell cross-sectional

shape. The shape depends, of course, on the magnitude of $\Delta P_{IL} = P_I - P_L$. While it remains elliptical two flow velocity profiles are required to define the flow pattern extremes. For laminar flow these are defined by

(1) the plane including and parallel with the major axis A at all x_i

$$U_A = \frac{\nabla P\ (r_A^2 - r_i^2)}{2\eta} \qquad (16a)$$

(2) the plane including and parallel with the minor axis a at all x_i

$$U_a = \frac{\nabla P\ (r_a^2 - r_i^2)}{2\eta} \qquad (16b)$$

The volumetric flow would then be

$$Q = \frac{\nabla P\ r_A^3\ r_a^3}{4\eta(r_A^2 + r_a^2)} \qquad (17)$$

It is evident that in a circular tube where $r_A = r_a$, (17) reduces to (4).

Complications arise, however, when the length of the constricted segment of L_c is too short for flow to become fully developed. Where R_e is high enough one could obtain values for U_m by applying the Bernoulli form of the continuity equation

$$P_1U_1 = P_2U_2. \qquad (18)$$

But one cannot obtain a realistic flow velocity profile from this relationship as $U(r_i) = U_m$ i.e. there is only particle velocity each at x positions 1 and 2 for the assumed frictionless fluid.

In short, the small compressed tube segment's slenderness ratio and its lack of axisymmetry present serious difficulties for

any fluid mechanics analysis. Shapiro (1977) in attempting to simplify the problem assumed that the collapsed segment was static and could be described by a "tube law" which relates segment cross-sectional area A to ΔP_{IL}. The need for a "tube law" in venous fluid mechanics should give one an appreciation of the difficulty in modeling the more complicated segmental or peristaltic constrictions to be discussed later; in these systems the 'collapsed' segment is travelling.

No velocity profiles are generated by the Shapiro model but two important parameters are presented which can be used to predict the general form of flow in a given collapsed vein.

(1) The speed index $S_p = U_m/c_o$ where if

$S_p > 1$, turbulence is likely
$S_p = 1$, choking (flow velocity falling to zero) is likely
$S_p < 1$, laminar flow is likely

(2) The 'shock wave index' (our term)

$$m = 3 + \alpha_T \frac{(\frac{d^2 f_T}{d\alpha_T^2})}{(\frac{df_T}{d\alpha_T})} \qquad (19)$$

where f_T is a tube law function such as $f_T = 1 - \alpha_T^{-1.5}$ which applies for thin-walled elastic tubes with $\alpha_T = A_c/A_o$, A_c the collapsed and A_o the uncollapsed tube cross-sectional area. If

$m > 0$, pressure pulse wave amplitude increases and wave valleys flatten
$m < 0$, pressure pulse wave amplitude flattens and wave valleys deepen

c. valves

Valves allow a number of veins, particularly those in the extremities to maintain flow against gravity. Consequently, where the body is horizontal the influence of venous valves on flow is

limited to their roles as 'roughness' factors of the walls. In contrast, venous flow velocity profiles developed from models which include valve-gravity interactions will have to include a term relating gravity to interstitial pressure, usually of the form

$$P_I = P_A + h_v \rho g \qquad (20)$$

where P_A is atmospheric pressure, h_v vertical distance below the point at which $P_I = P_A$ and g is acceleration due to gravity. There are apparently no fluid mechanical venous models which include valve effects on flow velocity profiles.

d. skeletal muscle compression

By increasing P_I, skeletal muscle in cooperation with venous valves acts as a pump auxillary to the heart. The assistance of skeletal muscle is not necessary for the horizontal body but is a prime factor in reducing blood pooling in the vertical body as indicated in Figure 6. By forcing the veins to 'collapse', skeletal muscle-pumps along a given vein create a kind of segmental constriction pattern which, if measured in a subject walking at a regular pace, may be a reasonable basis for constructing models which have the form of segmentation with valves superposed. Skeletal muscle venous pumps are an example of what we term "combination pumps" wherein a pumping mechanism which is not strictly part of the physiological tube in question has a significant affect on the tube flow-generating force.

2. Pressure effects

The role of pressure in macrocirculatory input flow has been refered to in the 'geometry' section but may be more explicitly summarized here as being threefold:

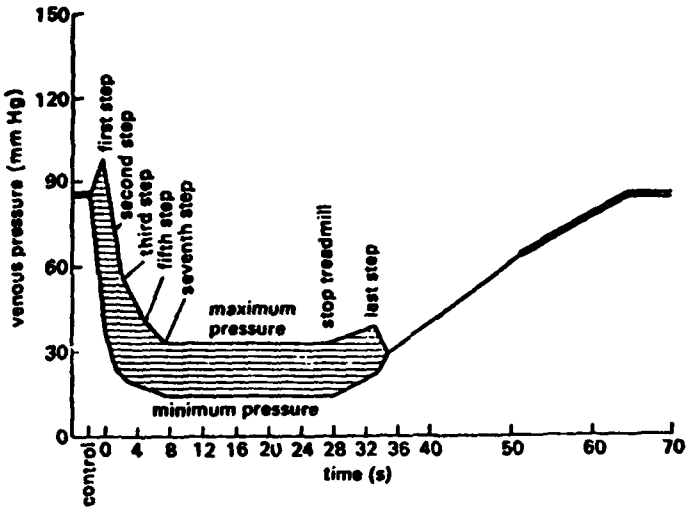

FIGURE 6

Effect of skeletal muscle contraction on venous flow. A combination pump system. Pressures are measured in an ankle vein of a subject who starts (at t=0) from and stops (at t=36) at a motionless erect position. From Pollack and Wood (1949).

(1) Transmural pressure ΔP_{IL} determines the geometry (within the constraints of vessel elasticity) of the vein.

(2) Given that net venous upstream pressures are below 20mm Hg, one can see that flow becomes extremely sensitive to changes in the axial pressure gradient ∇P. Thus just after the right atrium has emptied most of its contents into the right ventricle and before atrial diastole, P_L is at a minimum in the input chamber and the vein-to-atrium downstream pressure gradient is increased enough to cause a jump in flow. This 'pump-pull' effect is augmented by a 'pump-push' effect from the left ventricle during ventricular systole. Consequently, there are two U_m peaks in the venous system during the cardiac cycle.

(3) The form of the ventricular pulse must be considered separately from its ability to increase the the ventrical-to-vein downstream pressure gradient. The influence of tube geometry and elasticity on pulse wave amplitude and c_o as expressed in the Moens-Korteweg equation has been discussed. There are some important differences in the venous transmission of the wave. While reflection off flow dividers which is a dominant influence on pulse wave amplitude in the arteries is absent in the veins, the collapsed tube geometry, low-elastin wall composition and valve-based wall roughness provide sufficient mechanisms for altering pulse wave amplitude. Unfortunately, as one might expect from our description of the state of the art for the less complex output macrocirculation, there do not appear to be any fluid mechanical models which generate flow velocity profiles by relating c_o to $U(r_i)$ in the veins.

3. Viscous effects

Viscous effects in the veins are relatively constant as is the case in the larger arteries because vessel calibers are similarly large. In addition, the non-Newtonian rheology of blood probably has less affect on confluent flows because the walls are 'receding' radially. In collapsed tubes, however, where one might expect Newtonian rheology from high wall shear, there may be a sufficiently small a (minor axis) to produce non-Newtonian effects. Moreover, it is not clear how RBC's would migrate in these vessels. Unfortunately, all collapsed or circular tube venous flow theoretical models developed thus far assume a constant viscosity.

V. Ciliary Flows

1. General

The main pump for pulsatile flow is upstream. In contrast, ciliary tube flows are driven by numerous pumps, cilia, which are distributed over the lumen epithelium. Ciliated tubes occur in a variety of organs as indicated in Table 2. Unlike pulsatile flow ciliated tubes may generate "external flows". External flows differ from internal flows in that they are either bounded by a compressible fluid or at least half of the boundary parallel with U_o is too far away to measurably influence it. An example of an external ciliary flow tube is the trachea. The ciliary flow regime is in the low R_e range at all times as indicated in Table 3 and all ten assumptions used in the development of the Poisuielle model and listed in section III apply to current ciliary flow models. Consequently, all models presented are derived from some form of the Stokes equation. There are two levels, however, at which the models must operate

(1) Each pump is a slender body which moves a microvolume of fluid by oscillating and also interacts with other pumps. For this level flow may not be laminar but it is at a very low R_e and the Stokes equation applies in the slender body regime for $R_e \ll 1$.

(2) The additive effects of all the cilia in a field produce flow which is assumed laminar and therefore predictable from some form of the Poiseuille model.

In vertebrates cilia are generally 5-7 μm in length L_c and 0.2 μm wide $2r_c$ giving them a slenderness ratio, $L_c/2r_c$, of 25-35. They are arranged in arrays of rows and columns, the latter parallel to the flow axis as indicated in Figure 7. Cilia generate flow by periodically stroking in the downstream columnar direction at least twice as fast as their upstream or "recovery" stroke. Moreover, the downstream or "effective" stroke of this beat cycle is relatively stiff with the cilium fully extended while the recovery stroke exhibits considerable bending as the cilium tip stays relatively close to the epithelial surface.

Adjacent cilia in a row beat synchronously but those adjacent in a column beat slightly out of phase in such a way that as each cilium follows its neighbor to the maximum extension height, a wave appears to propagate up the column, i.e. in the upstream direction. The apparent wave is called a "metachronal wave" and the fact that it moves opposite to the direction of the effective stroke classifies it as an "antiplectic" metachronal wave. The metachronal wave velocity c_m is related to the beat frequency f by

$$c_m = f \lambda_c \qquad (21)$$

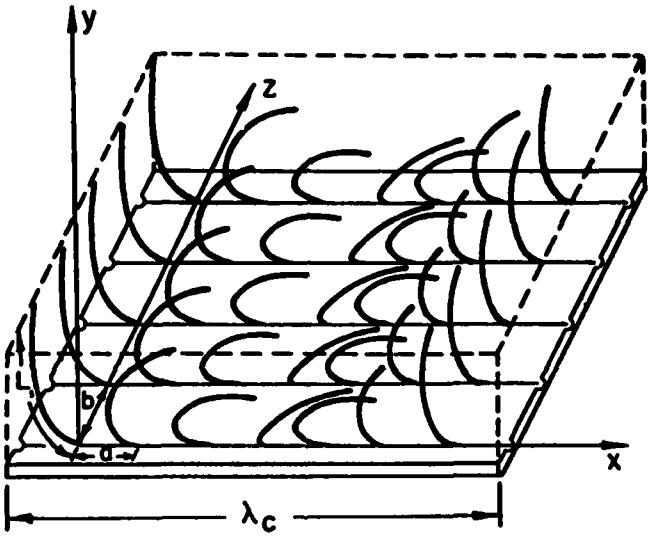

FIGURE 7

Array of cilia or ciliary field (from Keller et al, 1975). Columns run in the x direction with ciliary effective stroke toward the right and antiplectic metachronal way propagated toward the left. Rows run in the z direction to width L_E with synchronous ciliary beats. Sublayer thickness defined L_s in the figure and one metachronal wavelength λ_c defined by the dashed line in the x direction.

where λ_c is the metachronal wavelength.

The fluid mechanics of cilia has been reviewed in detail (Blake and Sleigh, 1974; Brennen and Winet, 1977) and we shall describe its main components.

a. Flow resulting from the motion of individual cilia

The large slenderness ratio and low R_e of cilia allow us to make some approximation about their cross-sectional geometry. We assume that instead of a tapered cylinder, the cilium is a string of spheres of radius r_c which acts like a cylinder. During an infinitesimally small increment of time dt each sphere exerts a force on the fluid equivalent to that predicted by Stokes Law:

$$F_{si} = 6\pi\eta U_{ci} r_c \qquad (22)$$

where U_{ci} is the speed of the cilium sphere at position i. The total force exerted by each cilium on the fluid during this time increment is not merely the sum of all its F_{si}'s because the direction of each F_{si} along the slender body must be included in the summation process which is in fact an integration of the forces distributed along the entire moving cilium. Accordingly, the motion of the entire cilium during dt must be defined. In addition, we cannot ignore the influence of the epithelial wall on the motion imparted to the fluid by the beating cilium.

In terms of its location as part of a slender body, Hancock (1953) defined a ciliary sphere (or point for purposes of integration) which generates F_{si} as a "Stokeslet" so in order to calculate the force exerted by a single cilium during dt one would have to integrate all the Stokeslets along the entire cilium. Furthermore, in order to calculate the force exerted by the cilium during

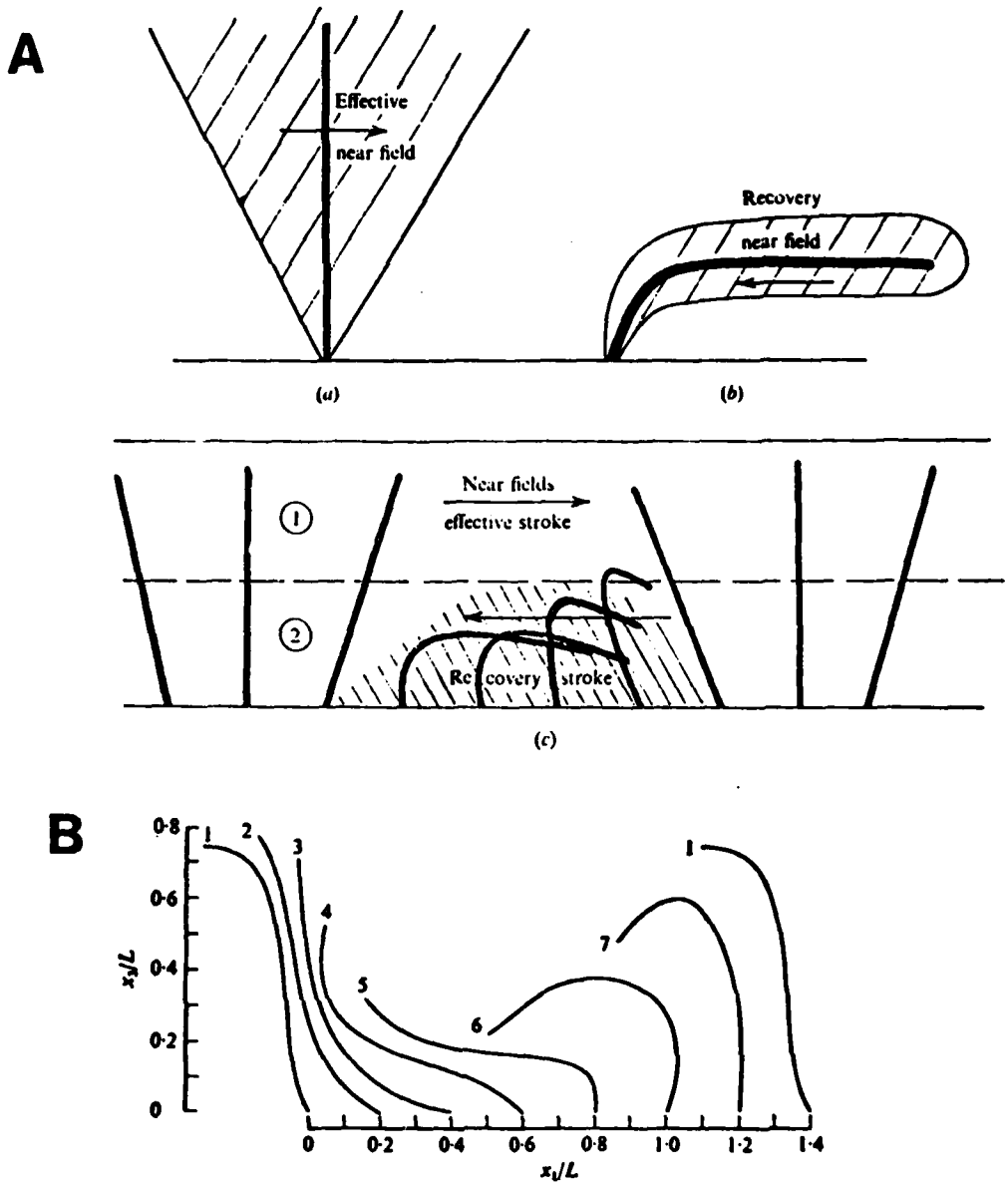

FIGURE 8

Two examples of mapping of ciliary motion through one beat cycle. A. Stokeslet field or integrated stokeslet region of influence mapped for the two extreme positions of the cilisary beat cycle (from Blake, 1972). (a) the Stokeslet field near the cilium during the effective stroke. (b) the field during the recovery stroke. (c) the 'layers' of principle influence during the ciliary beat cycle for the effective stroke (1) and for the recovery stroke (2). B. Computer-generated changes in ciliary form during one beat cycle as modeled by Liron (1978) to compute the net stokeslet filed. L = cilium length; x_3 = height above epithelium; x_1 = distance in ciliary column direction.

one beat cycle one would have to then follow the motion of each i through this cycle and integrate all the changes in position until all the dt's add up to one beat cycle period. An example of such cycle mapping is shown in Figure 8.

Gray and Hancock (1953) simplified the difficulties that these integrations presented by separating the directional components of ciliary force exerted by each of n cylindrical segments of cilia of length ds into

(a) a component tangent to the axial curvature of the segment dF_{cT} and

(b) a component normal to the axial curvature of the segment dF_{cN}.

These tangential and normal forces generate tangential and normal fluid flow velocities, U_T and U_N according to:

$$dF_{cT} = C_T U_T ds \quad \text{or} \quad \frac{1}{C_T} \frac{dF_{cT}}{ds} = U_T \quad (23a)$$

$$dF_{cN} = C_N U_N ds \quad \text{or} \quad \frac{1}{C_N} \frac{dF_{cN}}{ds} = U_N \quad (23b)$$

where C_N and C_T are velocity coefficients which contain viscosity terms and have a ratio C_N/C_T between 1.6 and 1.9.
The integration of 23ab has resulted in reasonably good predictions of the motion of self-propelled slender bodies such as spermatozoa.

Primarily because the Gray and Hancock model assumes the slender body to be of infinite length, however, it has not been useful for modeling flow due to an array of cilia.

b. Flow resulting from the motion of ciliary fields

The Stokeslet force generated by a ciliary sphere decreases in

influence from the surface of the cilium outward to F_{cd}. The decrease pattern as measured in an "unbounded" fluid goes like

$$F_{cd} = F_{si} r_c / d \qquad (24)$$

where d is distance from the cilium axis (It will be noted that on this axis F_{cd} is infinite. This is why a Stokeslet is classified as a "singular" force; i.e. it forms a "singularity" at d = 0). The distance between ciliary bases (at i = 0) along a column is about 0.5 μm. The interciliary distances at other i's will vary particularly at the tips but we can estimate the order of the influence of one cilium on another as $O(F_{cd}/F_c)$ = (0.2/0.5) x 100 = 40%, i.e. each cilium 'feels' about 40% of the Stokeslet value at the surface of its columnar neighbor cilium.

Of course any cilium in an array interacts with more than one neighbor. It is influenced by its other nearest columnar neighbor and its two nearest row neighbors as is evident from Figure 7. As may be appreciated, the integration of all these interactions and the influence of the epithelial wall at which the no slip condition must apply is quite a bit more difficult than the problem treated by Gray and Hancock (1955).

Blake (1972) assumed an infinite array above which there is no boundary and performed this integration of Stokeslets over a cilium directly using the ingenious device of a Green's function to solve the integral. The solution is, however, numerical and, consequently, not of a form into which Physiologists can 'plug in' measured values. Moreover, although Blake's solution was a major advance, the matching up of local flow generated by each cilium with resultant periciliary (within the sublayer between the cili-

ary tips and the epithelial base) flow was mathematically intractable so the model was limited to an expression for a "mean velocity field" $\bar{U}(y)$, where y is height within the ciliary sublayer. The numerical method averaged the contribution of each cilium to the net fluid flow over a beat cycle.

In an attempt to recover any details lost by Blake's averaging method, Keller et al (1975) developed a "Traction layer" model which follows the force generation by individual interacting cilia contained in one λ_c. The authors assume the same boundary conditions and integrate all the dt's, i.e the contributions of each of the cilia in the defined field during one beat cycle and term the results a "volume force". The periciliary flow field, termed an "interaction velocity" field, was then obtained by numerical integration.

Accordingly, while both methods developed models for periciliary flow, they were not in forms amenable to testing by plugging in physiological data. Moreover, their assumption of an unbounded surrounding fluid makes them of limited application for predicting tube or other internal flows.

2. Pressure effects

It may seem inconsistent that a flow velocity profile can be generated from an integration of a distribution of Stokeslets in space and time; particularly since there is no pressure term in Stokes Law (22) or the Gray and Hancock model (23ab). The simple explanation is that (22) is just one side of the Stokes equation (5) with $F_{si} = F_v$ which is balanced by the pressure gradient. But the relationship $F_v = F_p$ does not give us any expression for the

form of the pressure stress and, therefore, cannot describe its contribution to the flow velocity profile. Indeed, inclusion of pressure terms in the Keller et al model would probably have increased its complexity beyond the limits of the Stokes equation because the terms would have been oscillatory, greatly increasing the local R_{ef} value and subsequent evaluation of cilia interactions.

The main reasons that in spite of the pressure term omission, a flow velocity profile could be obtained by the Blake and Keller et al models are that the

(1) fluid is assumed unbounded above

(2) flow velocity profile calculation extends very little beyond the sublayer

(3) ciliated surfaces modeled are self-propelling (non-stationary).

In the real world, of course, there are boundaries and at some point the flow profile above the sublayer will have to be calculated.

For self-propelling bodies these corrections present few problems as long as the boundaries are reasonably far because the penetration of the disturbance caused by the body falls off like a Stokeslet. For stationary ciliated epithelium the unbounded solutions apply if the overlying liquid is bounded by a gas and the side boundaries are far enough apart. These fluid systems are, of course, external flows and, consequently, exclude any stationary boundary at which pressure generated by the additive effect of all cilia can build up. The cilia of lung epithelium are commonly modeled as external flow generators but as we shall show there are circumstances when they may generate internal flows, i.e. they are bounded in such

a way as to allow pressure generated by the pump to build a gradient.

Internal flow ciliary systems may develop significant downstream pressures. Morris(1981) has obtained a measurement of 2.3 mm Hg from the ciliated funnels of toad kidney. The most straightforward response to the need to include a pressure term in an internal flow ciliated system has been to impose a 'reasonable' pressure gradient along the system flow axis. Then one simply superposes (adds together) the calculated flow due to the imposed gradient and the periciliary flow generated by the resistive force-based ciliary model to obtain a "matched" flow velocity profile. We refer to pressure obtained in this manner as "implicit" pressure because while no connection between it and the cilia has been derived formally, it must exist if the internal cilia are pumping an incompressible fluid and mass is conserved.

The most physiologically useful result of this approach has been the Blake (1973) model for liquid pumping by a ciliated tube whose velocity profile equation has been presented in (7). In this model Blake matches the maximum fluid particle velocity generated near the ciliary tip U_m as computed from the sublayer model (Blake, 1972) with a Poiseuille flow profile generated by an implicit pressure gradient which rises in the downstream direction. The attraction of this model rests with the relative ease with which a Physiologist can plug in measured values for U_m and ∇P and predict the resultant flow velocity profile or U_m and U_o and predict ∇P from the same model. A comparison of an appropriate form of the quantitative model with measured flow in a ciliated channel (Winet and Blake, 1980) is presented in Figure 9. The volumetric flow

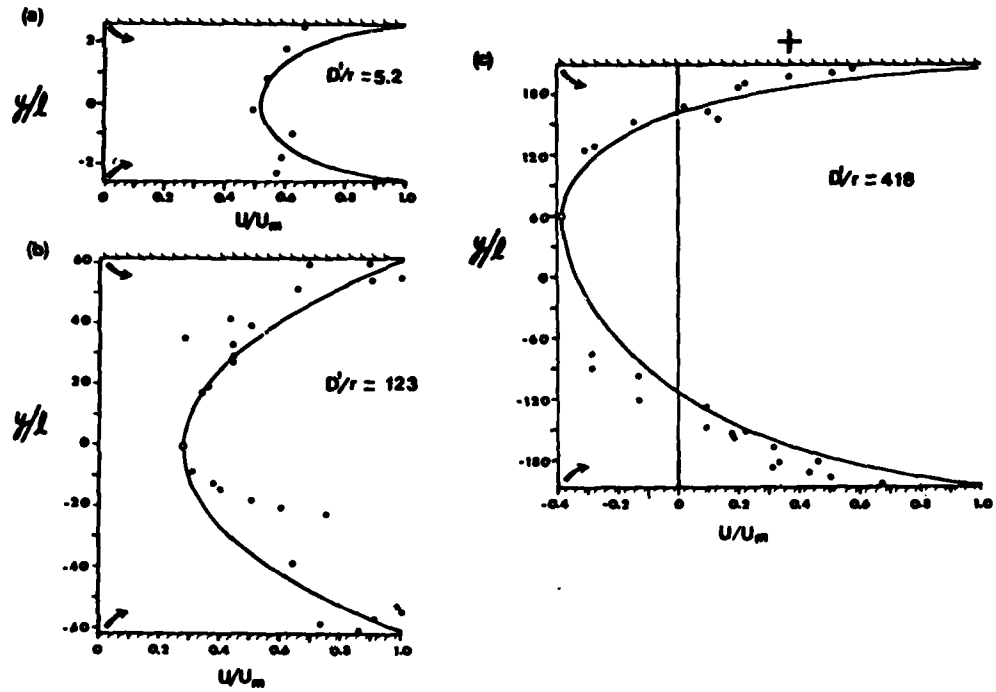

FIGURE 9

Comparison of data with model of Blake (1973) applied to a ciliated channel. Flow velocity profile is obtained from equation (26) and data points from a frog palate experimental model (Winet and Blake, 1980a).

rate for the tube model is given by

$$Q = \frac{\pi r^2 U_m}{2} - \frac{\pi r^4 \nabla P}{8\eta} \qquad (25)$$

As is the case for equation (15) this model allows for cancellation of flow due to ∇P by that due to U or vice versa. Thus, although the source of these two quantities is different their interaction may be expressed mathematically by similar models.

Recent attempts to obtain a explicit pressure term in the flow velocity profile for ciliated tubes have been spearheaded by Liron and his colleagues (Liron, 1978; Liron and Mochon, 1976; Liron and Shahar, 1978) but no exact solutions (ones into which measured values may be plugged directly) have been obtained.

3. Viscous effects

a. Mucus

All ciliated epithelia reported thus far have been found to contain periciliary glycoprotein which varies in concentration from the less than 1% (w/V) in the brain ependyma to as much as 10% in the non-ovulatory cervix. These mucin suspensions tend to display highly non-Newtonian behavior at ciliary shear rates to concentrations at least as small as 1.7% (Winet, 1976). The rheological effects are a function of concentration and relatively independent of the source of mucin (McCall et al, 1978). Thus one may directly apply mucin viscometric results from one organ or organism to another in developing experimental models.

There appear to be no models for internal ciliary tube flows of non-Newtonian fluids although the experiments of Yates et al (1980) to determine the ciliary shear stress on a sputum plug provide some useful data for such a model. External mucociliary systems have been modeled assuming the mucus blanket to be a merely more viscous Newtonian liquid, with recent versions stressing the role of the penetration of ciliary tips into the mucus layer as a

key to the propulsive mechanism (Blake and Winet, 1980; Yates et al, 1980). But more recent results (Winet et al, 1982) suggest that there exist mucus blankets which rest on a column of fluid thicker than the ciliary sublayer. There is a model (Ross and Corrsin, 1974) which contains these general features and includes a viscoelastic term for the mucus. But this model does not address periciliary flow.

If the mucus boundary is sufficiently rigid it may act as an overlying wall, thereby converting an external to an internal flow system. The physiological implications of an internal flow system beneath the mucus blanket are significant. It has been demonstrated that external cilia create sufficient stirring to reduce the unstirred layer and enhance transmural transport (Nelson and Wright, 1974). It has also been shown that internal ciliary flow systems show no local reflux if r is small enough (Winet and Blake, 1980). Thus, a submucal periciliary flow system may exist <u>in vivo</u> which would be analogous to capillary flow in coupling bulk and transmural flows--i.e. a combination pump system.

b. Spermatozoa

The efferent ducts of the male accessory tract are lined with cilia. So are the cervix, uterotubal junction and ampulla of the female tract. While the latter tube also carries the ovum, we shall not consider its transit as it is usually not treated as a liquid. All of these tubes do, however, transport spermatozoa which present two kinds of rheological problems depending upon their motile state.

In the efferent ducts spermatozoa are not motile and the vis-

cosity of their suspension may be modeled by an adaptation of the Einstein equation similar to that for RBC's (Winet, 1980a). In contrast, spermatozoa in the female tract are self-propelling and while there is evidence that they are oriented by the flow of the continuous phase (Roberts, 1970) the contribution of their self-oscillation to suspension rheology is beyond current modeling methods.

4. Geometric effects

Ciliated tube geometry may deviate significantly from a circular cylinder and those that do not are not infinitely long. Accordingly, entrance and exit effects will have to be included in the simplest realistic models while bends and branching will have to be added for such tubes as efferent ducts and bronchioles; and taper for the oviduct (Blake and Vann, 1982). Where cross-sectional geometry is not circular as exemplified in Figure 10 some rather complex functions of r_i will have to be introduced.

Two examples of geometric adaptations of the Blake (1973) model may serve as illustrations of geometric effects.

(1) Where a tube is replaced by a channel with all other boundaries much farther from the channel center that the ciliated epithelium we have

$$U(r_i) = \frac{U_{m1} + U_{m2}}{2} + R_{ci}(U_{m1} - U_{m2}) - \frac{\nabla P}{2\eta}((r - L_c)^2 - r_i^2) \qquad (26)$$

where $R_{ci} = \frac{r_i}{r - L_c}$ and U_{m1} and U_{m2} are differing U_m's for each epithelium and

$$Q = 2L_E(r - L_c)(U_{m1} + U_{m2}) - \frac{2\nabla P(r - L_c)L_E}{3\eta} \qquad (27)$$

where L_E is the thickness of the channel (i.e. epithelium). If we allow the open sides above and below the channel to be replaced by

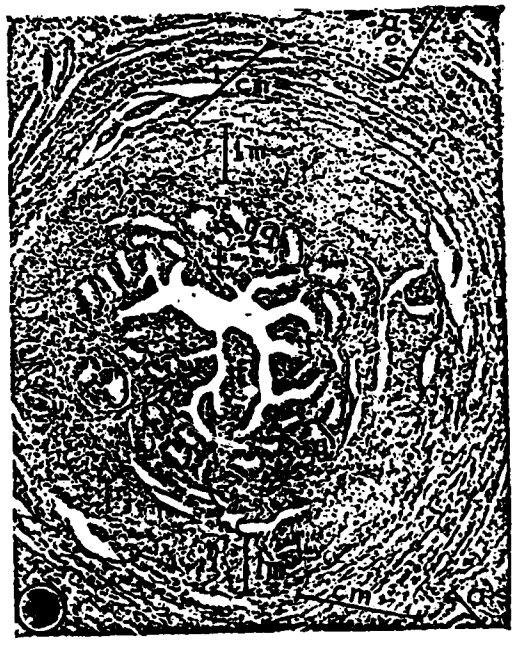

FIGURE 10

Ewe fallopian tube as example of the complex geometry which can be assumed by ciliated tubes (from Hook and Hafez, 1968). This is a cross section of the isthmus. Average width of lumen is about 100μm. Reflux is unlikely in smaller tubes. lm = longitudinal smooth muscle layer; cm = circular smooth muscle layer.

rigid boundaries L_E apart, a 'three-dimensional' channel is formed and we have

$$U(r_i) = \frac{(r-L_c)^2\nabla P}{2\eta}\left[1 - R_{ci}^2 - \frac{32}{\pi^3}\sum_{n=0}^{\infty}\frac{(-1)^n\cos(\pi R_{ci}(n+\tfrac{1}{2}))\ \cosh(\pi R_{cj}(n+\tfrac{1}{2}))}{(2n+1)^3\cosh(\frac{\pi R_{cj}}{R_{Ei}}(n+\tfrac{1}{2}))}\right]$$

$$+ \frac{2(U_{m1}+U_{m2})}{\pi}\sum_{n=0}^{\infty}\frac{(-1)^n\cosh(\pi R_{Ei}(n+\tfrac{1}{2}))\cos(\pi R_{Ej}(n+\tfrac{1}{2}))}{(2n+1)\cosh(\frac{\pi R_{Ei}}{R_{ci}}(n+\tfrac{1}{2}))}$$

$$+ \frac{2(U_{m1}-U_{m2})}{\pi}\sum_{n=0}^{\infty}\frac{(-1)^n\sinh(\pi R_{Ei}(n+\tfrac{1}{2}))\cos(\pi R_{Ej}(n+\tfrac{1}{2}))}{(2n+1)\sinh(\frac{\pi R_{Ei}}{R_{ci}}(n+\tfrac{1}{2}))} \qquad (28)$$

where $R_{cj} = \frac{r_j}{r-L_c}$, $R_{Ei} = \frac{2r_i}{L_E}$ and $R_{Ej} = \frac{2r_j}{L_E}$ with r_j the distance from the flow axis toward the non-ciliated (rigid) walls and L_E not only the epithelium thickness but the distance between the two rigid walls and

$$Q = \frac{U_{m1}+U_{m2}}{10} - \frac{(r-L_c)^2\nabla P}{8\eta} + \frac{2(r-L_c)}{15} + \frac{2^7(r-L_c)^2}{\pi^5}\sum_{n=0}^{\infty}\frac{\tanh(\frac{\pi}{5(r-L_c)}(n+\tfrac{1}{2}))}{(2n+1)^5}$$

$$+ \frac{16(U_{m1}+U_{m2})}{50\pi^3}\sum_{n=0}^{\infty}\frac{\tanh(5\pi(r-L_c)(n+\tfrac{1}{2}))}{(2n+1)^3} \qquad (29)$$

This model is due to Blake (personal communication) and one can obtain reasonable accuracy carrying the series to n = 10.

In closing this section we should like to stress again one of

the flow consequences of complex ciliated tissue geometries which create regions where r is small. If one of these regions is coupled with a region of large r such as is suggested by the vessel shown in Figure 10, a circulation will develop wherein reflux dominates the larger lumen and liquid is returned in the smaller lumens. This circulation has been suggested as a mechanism for spermatozoon transit in the female tract (Winet, 1980b).

VI. Peristaltic/Segmental Flows

Tubes which propel liquids by constriction owe their deformation to the contraction of smooth muscle. This tissue is found in a variety of tubes as indicated in Table 2. Its arrangement into circular layers is the basis for tube constrictions. A large number of electromyographic measurements of circular smooth muscle have been obtained from at least the GI and reproductive tracts but detailed measurements of contractile patterns have been rare and in no case have they been quantitatively related to flow. Moreover, there are apparently no measurements of flow velocity profiles for any smooth muscle tube.

1. Geometric effects--Due to the change in vessel shape being the basis for propulsion in these tubes, geometric effects are inseparable from kinematics (that aspect of physical analysis which describes motion without accounting for forces. Dynamic descriptions such as F=ma account for forces.)

The main obstacle to modeling smooth muscle tubes is that they combine the most complex dynamic qualities of pulsatile and ciliary pumping. Their pumps change tube shape at least as much as does cardiac muscle and their distribution, like ciliary systems, is all

along the tube.

In addition the constriction pattern is often irregular in form if not in time. For example, the constrictions may appear to repeat at the same tube position x_i forming a pendular wave which along one longitudinal line in the wall (+) and its opposite (-)(180° around the lumen) takes on the form

$$r(x,t) = \pm(r + H_1(x,t)\sin kx + H_2(x,t)\cos kx) \quad (30)$$

where $H_1(x,t)$ and $H_2(x,t)$ are functions allowing for change in amplitude with time at x_i from a sine wave to a cosine wave and $k = 2\pi/\lambda_p$. The pattern modeled by (30) is the classical segmentation pattern described by Cannon (1911) and shown in its in vivo form in Figure 11. Or the constrictions may propagate according to

$$r(x,t) = \pm(r + H \sin(kx - \omega t)) \quad (31)$$

where $\omega = 2\pi f$, which is the travelling sine wave characteristic of peristalsis modeling. Both of these kinematic models are highly simplified since in vivo the waves

(1) may be singular or otherwise non-periodic in incidence

(2) may not be sinusoidal in geometry

(Macagno and Christensen, 1981). Thus, it is probably more reasonable to think of these constriction movements as travelling sphincters.

The current state of smooth muscle tube modeling has not advanced sufficiently to generate exact solutions for wave forms more complex than sine waves. Indeed, there have been very few numerical solutions for tube motion beyond sinusoidal peristalsis because of the difficulties presented by the high degree of tube deformation. Among the non-sinusoidal models we may note that of

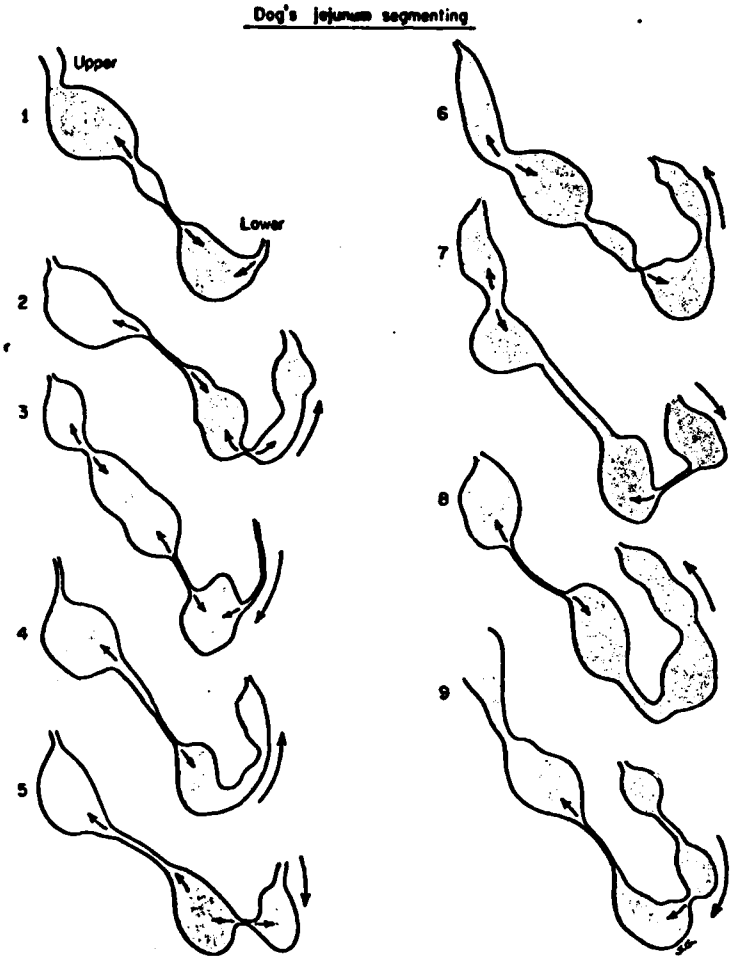

FIGURE 11

Segmentation in the dog jejunum. Arrows show direction of flow of barium sulfate suspension as recorded by X-ray cinematography. Interval between successive tracings is one second. From Davenport (1977).

Macagno and Hung (1967) which attempts to model the propulsion of a bolus in the form of a vortex doughnut (Singerman, 1974). These equations, being numerical, are not in plug-in form.

Let us look closer at the tube deformation problem. In all tube flow models we have examined in the present review, flow has been one-dimensional, i.e. laminar or parallel with the tube axis. Thus if one drew an imaginary line parallel with the tube axis--a "streamline"--and could identify each fluid particle that entered or left this line, they would find that the only particles that did so were at the ends. If all the streamlines at one particular distance r_d from the axis were drawn (an infinite number in theory) they would form an imaginary tube--a "stream tube"--concentric inside the flow tube. If fluid particles left their streamlines but not their stream tubes we would still have laminar flow but now two-dimensional. When tube shape deviates from a circular cylinder, streamlines may deviate from being parallel with the flow axis but as long as fluid particles do not change stream tubes, flow remains laminar. Once fluid particles begin crossing stream tubes we have secondary or unsteady flow to which we cannot apply the Poiseuille model. At present fluid mechanical modeling of physiological tube flows has produced no exact solutions beyond laminar models which have been remarkably successful for tubes, like those of the pulsatile (non-pump) and ciliary systems, whose walls do not significantly change their geometries with time (Not even collapsed veins have been so modeled while collapsing.)

Since propagating constrictions are the only smooth muscle tube contraction patterns which have been fluid mechanically model-

THEORETICAL MODELS FOR PERISTALTIC PUMPING IN TUBES

REFERENCE	Φ	k_r	Re	ΔP_λ	f	Inertial	Newt.Fl.?	End Condtn
Barton & Raynor (1968)	small	sine,small	0	avg. 0	?	no	yes	no
Burns & Parks (1967)	small	sine,small	0	avg. 0	?	no	yes	no
Gupta & Seshadri (1976)	small	sine,small	$\ll 1$	varies	arb.	no	yes	no,taper
Jaffrin & Shapiro (1971)	small	sine,small	0	Poislle	arb.	no	yes	no
Lew, Fung & Lowenstein (1970)	arb.	nodal,arb.	$\ll 1$	local vs reservr	arb.	no	yes	reservoirs
Li (1970)	?	sine,small	?	avg.ind. of r	small	yes	yes	no
Liron (1976)	arb.	arb.	$\ll 1$	defined	?	no	yes	no,noted
Lykoudis & Roos (1970)	?	arb.	$\ll 1$	avg. 0	?	no	yes	no
Manton (1975)	arb.	sine,small	1	max. P	small	yes	yes	no
Shapiro, Jaffrin & Weinberg (1968)	arb.	sine,small	0	external	0	no	yes	no
Shen (1976)	arb.	sine,small	1	defined	arb.	yes	yes	no,x-sect. arb.
Tong & Vawter(1972)	arb.	sine,arb.	$\ll 1$	implicit	?	no	yes	no
Yin & Fung (1969)	small	sine,arb.	≤ 100	ϕ depend.	?	yes	yes	∇P only

Table 4

ed we shall concentrate on peristalsis. When fluid mechanicists were drawn in large numbers to peristalsis modeling in the late 1960's by the problem of how bladder infections could spread to the kidney when reverse peristalsis in the ureter does not normally occur (Lapides, 1976), they determined that the most tractable model would eliminate either the tube wall motion or the particle motion. Thus, if they could not assume a constant geometry like those modeling collapsed veins, they would try to avoid having to account for both fluid particle and wall radial motions. This goal is accomplished by establishing either the wall at some point as being the fixed reference frame--the Eulerian system--or each fluid particle as being the fixed reference frame--the Lagrangian system. Macagno and Christensen (1981) deal in considerable detail with this approach. Unfortunately, the resulting models have not been particularly useful for physiologists because of the lack of plug-in results cited above. A sampling of the kinds of approaches engaged in by these modelers is presented in Table 4. Nearly all of them assume either a R_e or a constriction too small. In addition, a plemic has developed (Jaffrin and Shapiro, 1971; Yin and Fung, 1969) about the technique of applying the two frames of reference.

The one model which has resulted in an exact solution is that of Shen (1976; and Shih, 1978). He bypassed the entire Eulerian -Lagrangian problem by choosing the lab frame as his fixed reference. Although complex in scope the Shen model, which is presented in equation (8), is ideal for plugging in quantitative measurements. More recent complications of the Shen model have led to numerical models (Shen et al, 1980) so we shall not deal with them.

Since there have been no reported flow velocity profiles for peristaltic or segmental tubes there are no data points to test a plot of (8). Accordingly, as an exercise in testing we have plotted the fully integrated model,

$$\bar{Q} = \frac{\pi c_p A}{8}\left[8 + 4\phi^2 - \frac{8(1-\phi^2)^{-1.5}}{(1+1.5\phi^2)(1-\phi^2)^{-3.5}} - \frac{\Delta Pr}{c_p \eta (1+1.5\phi^2)(1-\phi^2)^{-3.5}}\right] \quad (32)$$

where each symbol was described for (8), for an efferent duct with two measured pressure gradients marked with vertical lines and average volumetric flow rates marked with horizontal lines. The plot is shown in Figure 12. Unfortunately, peristaltic waves have not been reported for these tubes which are extremely difficult to access; although their electromyographic acitivity has recently been measured (Talo, 1981). Efferent ducts and oviducts also carry cilia and so qualify as combination pumps.

a. In vivo peristalsis

Peristalsis has been measured primarily in three tubes, the ureter, esophagus and colon. It has also been observed in the small bowel where it functions as a "housecleaner".

The ureter is about 30 cm long and 0.2 cm in caliber which progresses from a stellate to a circular cross-sectional lumen geometry as the lumen distends (Lapides and Diokno, 1976). As with other smooth muscle tubes the length is not constant due to the contractility of the longitudinal smooth muscle layer. If it were a rigid tube the ureter's slenderness ratio would be sufficient to allow flow development (see Table 3) but the entrance length calculations are surely more difficult for peristaltic flow. The waves

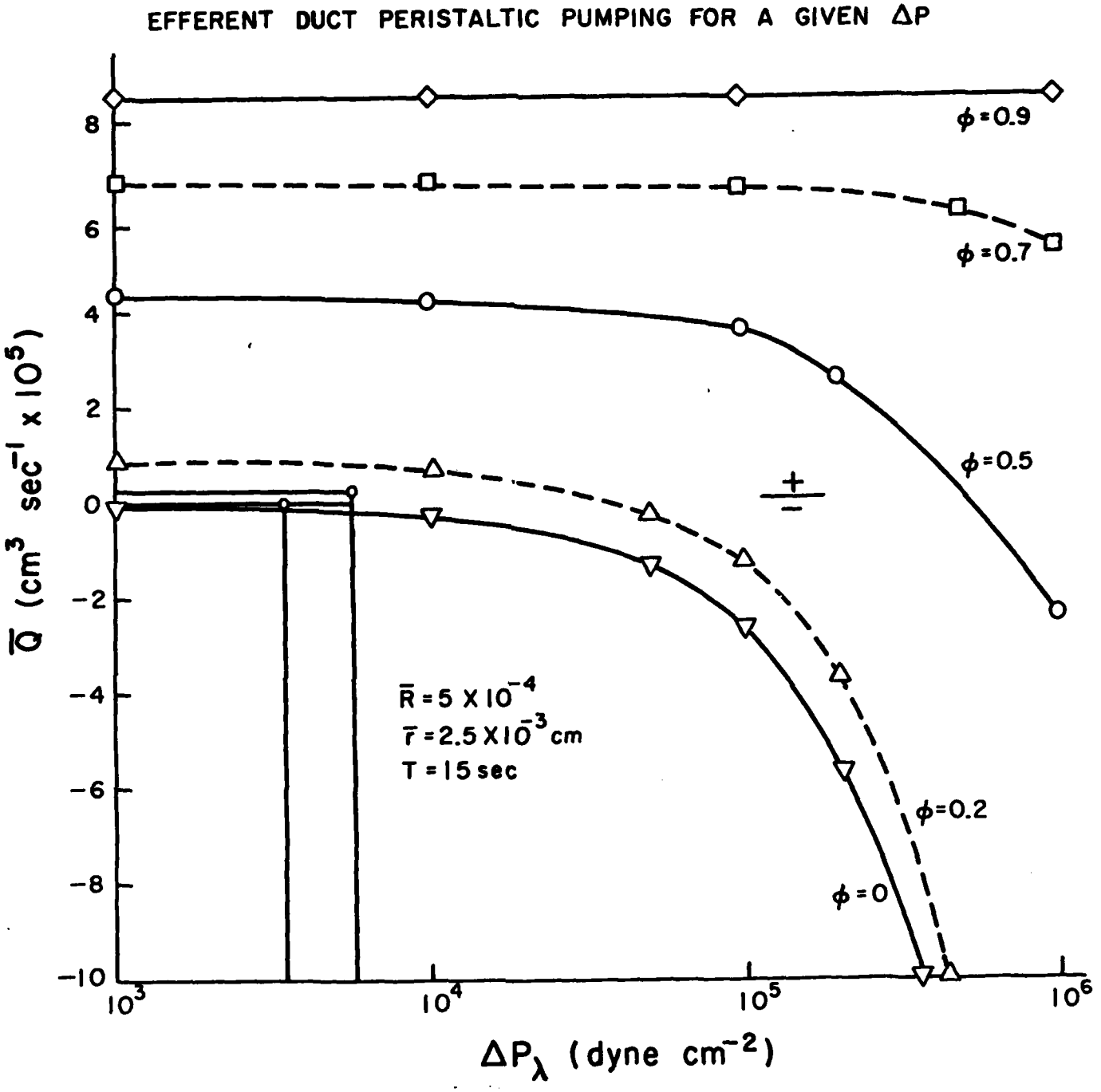

FIGURE 12

Shen (1976) peristalsis model applied to an efferent duct. Average volumetric flow rate $\bar{Q}$ is plotted as a function of pressure drop per wavelength for various values of ϕ. Range of measured values is indicated by open circles.

pass down the tube at about 3 cm/sec and there are rarely more than two present (Boyarsky and Weinberg, 1973). Other kinematic characteristics of the flow are summarized in Table 3. The shape of the uretral peristaltic wave is easily modeled by a single axisymmetric version of (31) (i.e. around the tube). The occlusion ratio ϕ is about 1 (We use 0.96 in the Shen model because, being asymptotic, it is singular at 1). The dilated region or bolus is about 5 cm long but the wave length is 6-9 cm including the $\phi = 1$ segments (Boyarski and Weinberg, 1973). A typical Q value for the ureter has been hard to obtain in spite of the existence of numerous cineradiographs primarily because the volume of stellate tissue cannot be subtracted from the X-ray images. A value of $Q = 0.02$ cm^3/sec is not, in any case, considered abnormal (Sokeland et al, 1973).

The esophagus is 25 cm long with a 2 cm caliber on the average. Propagation of liquid boluses occurs at an average of 4 cm/sec with some variation along the tube (Vantrappen and Hellemans, 1980). The vessel is flaccid while at rest but its inner geometry is sufficiently smooth that unlike the ureter, distension beyond simple filling is not necessary to make it circular in cross-section. Accordingly, it can be modeled as axisymmetric when carrying a liquid bolus. The tube has true sphincters at both ends which are coordinated by neural feedback loops. The upper or cricopharyngeal sphincter which is aided by skeletal muscle (Vantrappen and Hellemans, 1980) relaxes to accept the bolus and the gastroesophageal sphincter relaxes once the bolus is in the tube. As is the case in the ureter, the esophageal segments before and after

the bolus have $\phi = 1$. Also like the ureter, reverse peristalsis has not been confirmed in the esophagus. In contrast to the ureter, however, more than two boluses may exist in the tube simultaneously.

The colon is 150 cm long with a caliber averaging 4 cm. Its resting shape has a side-view accordian-like appearance with undulations called "haustra". Thus, this tube is not flat when empty. There are sphincters at both ends of the colon, the ileocaecal valve upstream and a series of sphincters downstream including one composed of skeletal muscle which is usually constricted. Peristalsis, consequently, which occurs about 50% of the time in this tube (Misiewicz, 1980), must usually push against a closed downstream sphincter. Accordingly, a significant amount of reflux (retropulsion) takes place in the colon. The peristaltic waves travel at about 2.5 cm/sec (Christensen, 1981). The existence of the haustra has made radiographic measurements of mass transit difficult, inhibiting the development of peristaltic models for the colon; however that of Picouloglou et al (1973) should be noted in passing. We should also note recent measurements of peristalsis in experimental models (Pescatori et al, 1980).

The small bowel normally exhibits peristalsis less than 5% of the time, using it to clear out chyme after processing, in response to a new meal or during phase II of the 1.5 hour cycle followed by the fasting human gut. Except for studies of abnormal episodes (e. g. diarrhea), small bowel peristalsis has not drawn much interest. Those modeling it, however, may have to be aware of longitudinal folds or rugae and the villi which line the lumen. These slender

bodies about 0.1 cm long and 0.02 cm wide oscillate at about 0.05 Hz and may contribute to wall "roughness" which would affect any boundary layer where flow is at high R_e. The small bowel also has numerous bends along its 640 cm length.

The stomach exhibits waves which appear peristaltic but it has such a small slenderness ratio and there is so much variation in the wave form between the antrum and fundus that it can hardly be called a tube in our sense. Moreover, it spends much of its time with the pylorus and gastroesophageal sphincter closed; generating considerable reflux. The uterus exhibits similar behavior giving these two vessels the most complex fluid flow of all body vessels.

b. segmentation

There is no apparent difference in relevant anatomy between tubes which propagate circular smooth muscle-caused constrictions over much of their length and those which do not. Thus, the latter seem to 'prefer' non-propagation. We arbitrarily classify a propagated constriction as peristalsis if it moves at least 2r. All others we place in the 'segmentation' category. There are apparently no quantitative kinematic descriptions of segmentation in non-digestive tubes although we should remark in passing that the oviduct appears to be the first which will break this ignorance barrier (Verdugo et al, 1980).

The small bowel tapers in caliber from 3.8 cm at the duodenum to 2.4 cm near the ileocaecal valve as it follows its 640 cm tortuous course. As indicated above the inner wall has a roughness due to villi and folds. The classic description of segmenta-

tion (Cannon, 1911) still holds although there have been refinements. The pendular pinching off which looks like shifting aneurisms oscillates at about 0.20 Hz in the duodenum. Oscillation frequencies then follow an aboral gradient--which is not strictly linear--down to about 0.16 Hz in the terminal ileum (Davenport, 1977) as shown in Table 3. While the constrictions do not propagate as peristaltic waves they do display an aboral 'shift' which results in a slow migration of the segmenting region up to 10 cm in the duodenum (Engstrom et al, 1979) and 15 cm in the rest of the small bowel. The speed of this migration also follows an aboral gradient from about 0.12 cm/sec in the duodenum to 0.025 cm/sec in the ileum (Grivel and Ruckebusch, 1972). Volumetric flow rates during segmentation also appear to follow a gradient from 2.1×10^{-2} cm^3 /sec in the jejunum to 8.3×10^{-3} cm^3/sec in the ileum.

Unfortunately, all the measurements cited in the last paragraph were not obtained from the same subjects. The unsteadiness of flow due to segmental contractions is certainly sufficient to prohibit lumping together of data. Moreover, there are in vivo variations of length of contraction and frequency at the same site (Weisbrodt, 1981) which make a Q predicted from just one pattern of segmentation of questionable applicability. From these considerations one would expect theoretical fluid mechanical models for segmental flows to be hard to come by and there are apparently none. But stochastic (statistical) models seeking to obtain at least a numerical form for the kinematics of small bowel motions are being developed, particularly by Singerman et al (1975) and Bertuzzi et al (1978). A related model has been developed for oviductal con-

traction patterns by Verdugo et al (1980).

2. Pressure effects

a. peristalsis

Pressures at the ends of peristaltic tubes are often independent of those produced by the propagating wave. In the ureter, an increase in urine formation which is linked to an increase in renal blood pressure causes an increase in renal pelvis volume. The reaction of renal pelvis smooth muscle to this volume increase, renal systole, generates a pressure increase at the proximal ureter of 5 - 10 mm Hg which stimulates the uretral peristaltic wave. The peristaltic wave pressure is characteristically about 15 mm Hg (Boyarsky and Weinberg, 1973), dropping to zero on each side of the urine bolus. Inserting these values and kinematic data cited above into the Shen (1976) model yields a $Q = 0.22$ cm^3/sec assuming a $\phi = 0.96$. This Q is larger than the 0.02 cm^3/sec cited above but falls well within the range of "spurts" into the bladder reported by Boyarsky and Weinberg (1973). Calculations from their data give a range of $0.007 \leq Q \leq 0.5$ cm^3/sec. In any case, small changes in ϕ, without reducing it below 0.90 will yield model values over the entire Boyarsky and Weinberg range which includes the Sokeland et al measurement. Uretral discharge into the bladder will not occur, however, if bladder pressure is too high. Reflux from the bladder is prevented by a "flap valve", the ureterovesical valve (Lapides, 1976). The volume of fluid in the renal pelvis and bladder also affects pressure via its response to gravity, flow being aided most while the subject is vertical. These relationships will have to be included in any model of uretral flow which includes end condi-

tions.

The pattern for initiation of peristalsis and pressure transmission in the esophagus is similar to that in the ureter although specific values differ. In this tube the lower valve is a sphincter instead of a flap valve. Also, deguttation (swallowing) creates highly variable entrance pressures. In particular the pharyngeal pressure wave hits the entrance of the esophagus at the cricopharynx with a pressure wave up to 6 mm Hg. Once the collapsed esophagus expands to accomodate the bolus it propagates a peristaltic wave at about 2 mm Hg (Henderson, 1980). Although the wave velocity averages 4 cm/sec it moves faster at the oral end because the first third of the tube is surrounded by skeletal muscle which contracts faster than smooth muscle. Another influence on lumen pressure is the diaphragm which controls thoracic cavity (the body cavity surrounding the esophagus) pressures and can create a considerable transluminal gradient. A rather delicate balance exists between the lumen pressures of the esophagus, gastroesophageal junction, stomach and thoracic cavity (Henderson, 1980) as shown in Figure 13. Thus, tube end conditions are a major factor in determining flow in the esophagus.

Another parallel between esophageal and uretral flow is the importance of gravity in determining net fluid motion. Liquids will usually precede their peristaltic wave to the stomach in an upright subject while solids are merely aided in their descent.

Pressure in the colon has been measured <u>in vivo</u> but not at specific sites along the tube and not in conjunction with peristaltic wave observations. The common form of manometry is a bal-

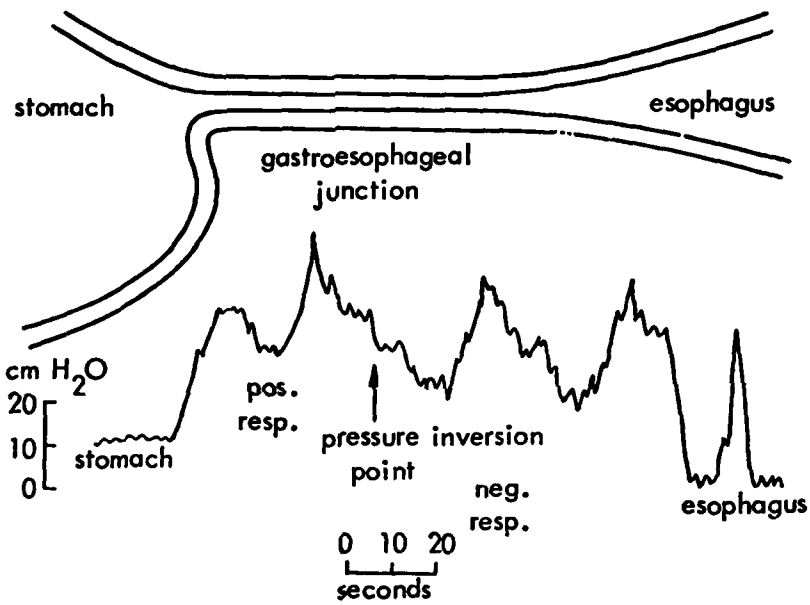

FIGURE 13

Pressures in the lumen of the lower (gastro-) esophageal junction during peristalsis resulting from the interaction of gastric, esophageal and thoracic pressures. PIP is a pressure inversion point resulting from negative thoracic pressure during inspiration. From Henderson (1980).

loon attached to a manometer. As evaluated by Christensen (1981) these colonic pressure measurements are of questionable reliability.

b. segmentation

Pressure measurements in the small bowel have progressed beyond luminal manometry in two directions. First, pressure transducers have been placed in vivo at intervals along the tube to give a much clearer picture of pressure distribution than luminal baloons can. Their measurements have shown that pressure changes may be limited to segments less than 2 cm in length (Weisbrodt, 1981). Pressures within a segmentation bulge may be as high as 50 mm Hg. As is the case for other smooth muscle tubes, the exit and entrance conditions determine the fluid content of the small bowel which is collapsed when not transporting chyme. Chyme enters the oral end of the small bowel through the pyloris, a long constriction 'valve' at pressures over 50 mm Hg. It leaves the 640 cm vessel to enter the large bowel through the ileocaecal junction at about 20 mm Hg. There is some disagreement regarding whether the junction should be considered a sphincter or valve (Weisbrodt, 1981). Second, the net pressure generation by a segment of small bowel is measured ex vivem by hooking up the vessel with fluid-filled tubes and determining the work performed moving the fluid against gravity (Weems, 1981; Weems and Seygal, 1980, 1981). Weems and Seygal (1981) found that 17 cm lengths of small bowel were capable of performing up to 9×10^4 dyne-cm of work. Given the length of the small bowel and the difficulty of keeping track of all the contractions at intervals at least as small as 2 cm (consider 321 chronically implanted

transducers), the ex vivem approach may be the most practical experimental model for testing fluid mechanical models.

3. Viscous effects

The restriction of most peristalsis models to the ureter is based in part on urine being a Newtonian fluid of viscosity 0.007 poise. In contrast the reproductive tracts move a non-Newtonian suspension of sperm and the female and GI tracts are lined with mucus. The stomach in particular has a 70% (w/V) mucus coating. In addition chyme and faeces are both highly non-Newtonian, even without the mucus coating they pick up from the tract walls. Notwithstanding these obstacles, colonic propulsion of faeces has been modeled numerically by Picologlou et al (1973) and Patel et al (1973) who represented faeces as a power law fluid. Even the water-like boluses in the esophagus cannot be considered strictly Newtonian as they usually trap some air during swallowing and tend to pick up strands of mucus as a result of mixing in the cricopharyngeal region.

The effect of mucus on boundary conditions must also be addressed by any complete model of smooth muscle tube flow. This viscoelastic fluid may fill-in regions of potential roughness thereby aiding 'slip'.

4. Longitudinal muscle

We should not leave the subject of smooth muscle tubes without considering the role of the longitudinal muscle layer in the kinematics and dynamics of the tube. Contraction of this muscle can result in a 75% tube shortening. However, there is no basis for expecting all the longitudinal smooth muscle fibers at a gi-

ven x_i to shorten or relax simultaneously resulting in an axisymmetric event. Consequently, the tube may bend in addition to any overall change in length. Given the relative slowness of these changes as compared with peristalsis or segmentation, the longitudinal muscle effects would probably be of second order importance (Macagno et al, 1975).

VII. Combination Pumps

When two or more of the three classes of physiological flow pumps combine to generate flow in a particular tube the analysis of the flow becomes more difficult. The difficulties are somewhat overcome, however, if one can simply combine the two pump models. The reader may predict from our previous revelation of the limited applicability of the three pump models showcased, that few attempts have been made to fluid mechanically model combination pumps; and for the most part this prediction is borne out. In the brief discussion to follow we shall present some examples of combination pumps including two which have been modeled fluid mechanically.

A. Pulsatile-skeletal flow propulsion

This combination works to aid input macrocirculation as described previously. The dominant random feature of the system which confounds modeling is the lack of phase matching between the skeletal and heart muscle contractions. Thus, valves are needed to help maintain the flow. There do not appear to be any exact quantitative models for this flow.

B. Skeletal-Peristaltic/Segmental flow propulsion

The esophagus is the prime example of this pump combination which features skeletal muscle as the main flow generator in the

upper third of the tube. The main components of this system have already been discussed. There does not appear to be any interest in modeling such flows, but tubes with skeletal muscle sphincters, such as the colon are attracting attention because of their influence on pressure patterns upstream.

C. Ciliary-Peristaltic/Segmental flow propulsion

This combination pump appears almost exclusively in the reproductive tracts (It may be said to exist to a limited extent in the lungs. One could make the same statement with regard to a skeletal muscle(diaphragm)-ciliary combination.). In the female the two pumps occur in the cervix, uterus and oviduct while in the male they combine only in the efferent ducts. We have modeled the latter (Winet, 1980a) by superposing the Shen (1976) and Blake (1973) equations. The model must be considered a first approximation because peristalsis has not been observed in these tubes although the electrical activity associated with contractions has been measured (Talo, 1981). Moreover, if peristalsis does exist in the male, ducts, the value of δ would have to be small enough to allow such an exercise in linear manipulation as superposition. The results of the cilio-peristaltic model are presented in Figure 14.

D. Peristaltic/Segmental-Pulsatile flow propulsion

This combination pump is one example of a widespread phenomenon. Any contractile tissue creates internal pressures which must alter its own blood supply at least momentarily. The constriction of coronary vessels by heart contractions is a well-known occurance. In the small bowel where tonic contractions can last up to 8 minutes (Weisbrodt, 1981) the effect on local circulation may be sig-

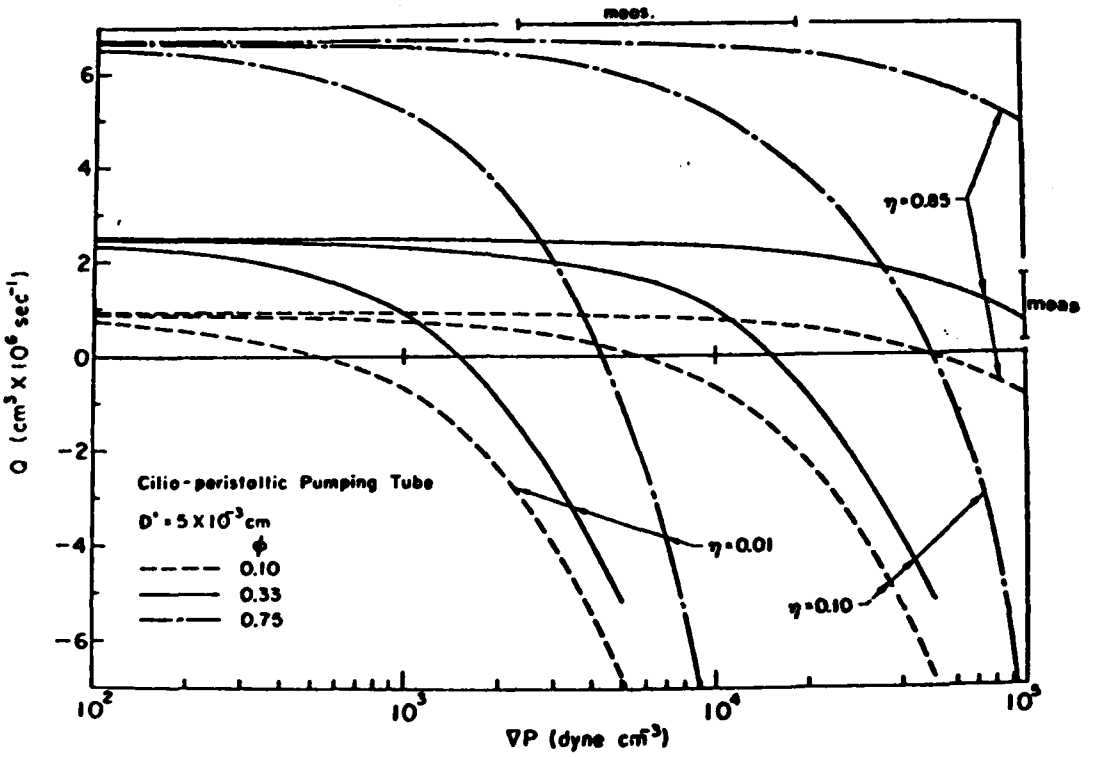

FIGURE 14

The combined effect of cilia and peristalsis on Q in a single efferent duct for various ϕ and η values as a function of ∇P. At low ∇P values, ϕ dominates Q but at high ∇P values η dominates Q. Measured ranges of Q and ∇P from experimental models are indicated by vertical and horizontal "error" bars respectively. From Winet (1980a).

nificant if it can be shown that the pressures involved are large enough. Swabb et al (1982) have found such an effect after raising intraluminal pressures in an ex vivem small intestine preparation to values well within the physiological range. They also found increases in secretion into and filtration out of the lumen. The feedback scheme proposed by these workers for the entire set of interactions is presented in Figure 15. A fluid mechanical model is the next logical step.

E. Pulsatile-Filtration flow propulsion

We have not dealt with convective flow through membranes because the tubes or pores do not have a clearly defined geometry. Filtration and its carrier version solvent drag, nonetheless are convective processes which are part of the most completely modeled combination pump. The solvent flow version was dereived by Starling, demonstrated by Landis and related to the fluid mechanical transport of solutes by Katchalsky-Curran (Lassen and Perl, 1979). The Katchalsky-Curran model which describes the interaction of pulsatile and oncotic pressures to bring about flux in a porous tube like a capillary is illustrated in Figure 16.

ACKNOWLEDGEMENTS:

The author wishes to thank Drs. M. C. Shen, J. R. Blake, G. J. Yates, P. Bass and T. Y. Wu for valuable discussions.

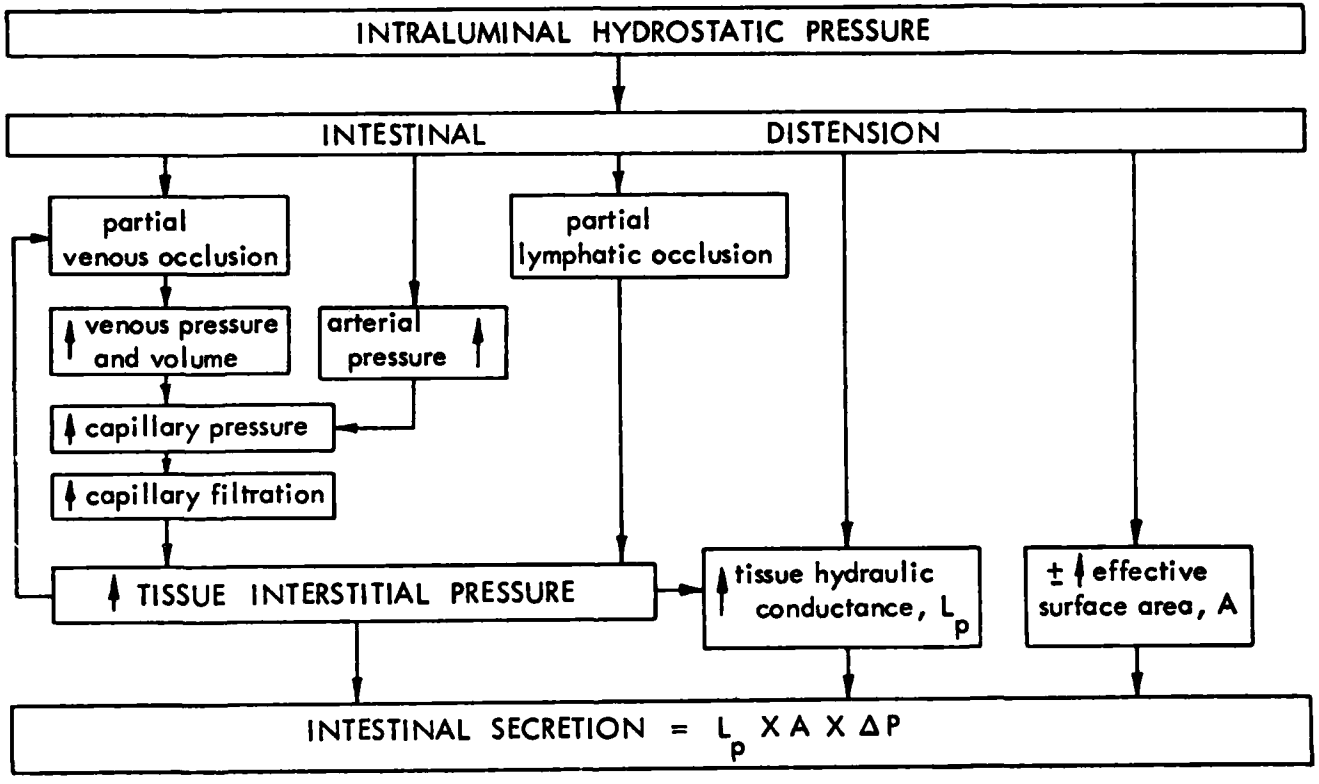

FIGURE 15

Proposed interaction of intestinal pressure with blood pressure and, consequently, blood flow as well as transmural transport (from Swabb et al, 1982). An example of a combination pump linking segmentation, pulsatile and filtration flows.

FLUID TRANSPORT THROUGH PORES IN CAPILLARY WALL

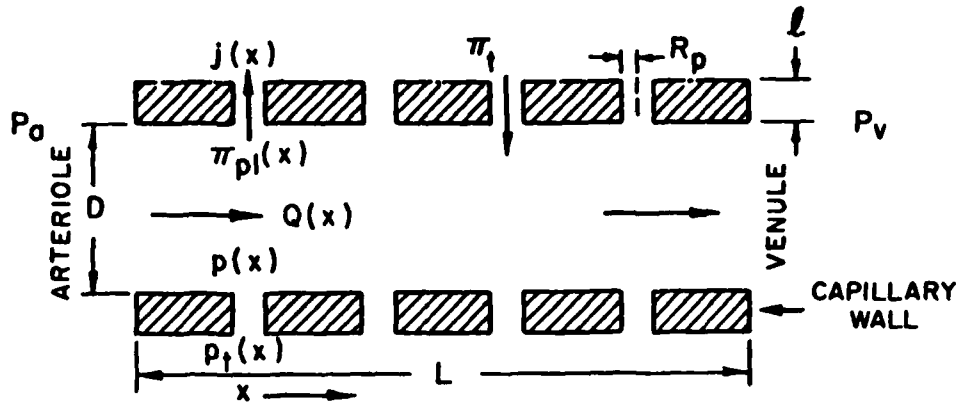

FIGURE 16

A combination pump linking pulsatile and filtration flows. The quantitative model describing transmural flux at a point x along the porous tube (e.g. capillary) is an extension of the Starling solvent flux equation to include solute flux:

$$j_s(x) = \omega(x)RT\Delta C(x) + \frac{1}{2} j_v(x)(C_o(x) + C_1(x))(1 - \sigma_v(x))$$

where

$\omega(x)$ = membrane permeability coefficient = $\frac{j_s(x)}{S\Delta C(x)}$ when $j_v(x) = 0$

S = area of membrane involved

$\Delta C(x)$ = transmural solute concentration difference = $C_o - C_1$ at x

R = gas constant

T = temperature

$\sigma_v(x)$ = solvent drag coeffcient = $1 - \frac{2j_s(x)}{(C_o(x)+C_1(x))j_v(x)}$ when $\Delta C(x) = 0$

$$j_v(x) = -L_p(x)[(p(x) - p_t) - \sigma_s(x)(\pi_{p|}(x) - \pi_t)]$$

where

$L_p(x)$ = filtration coefficient (hydraulic permeability) at x, = $\frac{\pi R_p^4(x)}{8\mu\ell(x)}$

$R_p(x)$ = pore radius at x

$\ell(x)$ = pore length at x

p(x) = plasma hydrostatic pressure at x

p_t = interstitial " "

$\pi_{p|}(x)$ = plasma oncotic pressure at x

π_t = interstitial " "

$\sigma_s(x)$ = reflection coefficient of solute at x, = $\frac{p(x) - p_t}{RT\Delta C(x)}$

SYMBOLS

a	tube caliber at constriction
A	tube cross-sectional area
c_p	peristaltic wave propagation velocity
c_m	metachronal wave propagation velocity
c_o	pressure pulse wave velocity
C_N	velocity coefficient normal to curvature of cilium axis
C_T	velocity coefficient tangential to curvature of cilium axis
D_u	Dean number
E	Young's modulus
f	frequency of pump oscillations
f_T	tube law function
$f(r_i)$	any function describing geometry only
F	force
F_g	force due to gravity
F_p	force due to pressure
F_s	Stokeslet or point force, a fundamental singularity of Stokes flow
F_{si}	Stokeslet at position i
F_v	force due to viscosity
h	volume fraction
h_v	vertical distance relative to gravity
h	amplitude
i	a whole number representing any one of a number of position
k	wave constant $2\pi/\lambda$
K	generally term for a proportionality constant
L	length
L_c	cilium length
L_E	epithelium width in the direction of ciliary rows
m	mass
$\mathfrak{M}$	shock wave index
P	pressure
P_I	interstitial pressure
P_L	tube lumen pressure
Q	volumetric flow rate

Q_b	volumetric flow rate in lubrication layer
r	tube lumen radius or one-half channel width
r_c	radius of cilium
r_i	distance from tube axis at position i
R_c	radius of curvature of tube axis
R_e	Reynolds number
R_{ef}	oscillatory Reynolds number
R_{et}	translatory Reynolds number
S_p	speed index
S_r	Strouhal number
U	fluid particle velocity
$\overline{U}$	average fluid particle velocity
U_{ci}	speed at position i of the cilium
U_N	fluid particle velocity component normal to curvature of cilium axis
$U(r_i)$	fluid particle velocity at position i along the tube radius
U_m	maximum fluid particle velocity
U_{m1}	maximum fluid particle velocity at one of two ciliated surfaces
U_{m2}	maximum fluid particle velocity at one of two ciliated surfaces
U_T	fluid particle velocity component tangent to curvature of cilium axis
$\overline{U}_T$	average particle velocity over one oscillatory period
U_r	particle velocity in the radial direction
U_{xi}	axial particle velocity at x_i
$U_{xi}(t)$	axial particle velocity at x_i as a function of time
U_o	axial fluid particle velocity at the tube axis
x_i	any one of numerous positions i in the x direction
y	distance from the wall in Cartesian coordinates
α	Womersley parameter
α_T	collapsed tube area ratio
ρ	density
ΔP	pressure drop
Δw	wall thickness
∇P	pressure gradient
η	viscous coefficient
η_o	continuous phase viscosity of a multiphase system

τ	tension
λ_c	metachronal wavelength
λ_p	peristaltic wavelength
ω	angular velocity

REFERENCES

Bagge, U., P.-I. Branemark, R. Karlsson and R. Skalak (1980) "Three dimensional observations of red blood cells in capillaries" Blood Cells 6: 231-236.

Batchelor, G.K. (1974) "Transport properties of two-phase materials with random structure" Ann. Rev. Fluid Mech. 6: 227-255.

Bergel, D.H. and D.L. Schultz (1971) "Arterial elasticity and fluid dynamics" Progr. Biophys. Mol. Biol. 22: 3-36.

Bertuzzi, A., R. Mancinelli, G. Ronzoni and S. Salinari (1978) "A mathematical model of intestinal motor activity" J. Biomech. 11: 41-47.

Blake, J.R. (1972) "A model for the microstructure in ciliated organisms" J. Fluid Mech. 55: 1-23.

Blake, J.R. (1973) "Flow in tubules due to ciliary activity" Bull. Math. Biol. 35: 513-523.

Blake, J.R. and M.A. Sleigh (1974) "Mechanics of ciliary locomotion" Biol. Rev. 49: 85-125.

Blake, J.R. and H. Winet (1980) "On the mechanics of muco-ciliary transport" Biorheol. 17: 125-134.

Boyarsky, S. and S. Weinberg (1973) "Urodynamic concepts" in W. Lutzeyer and H. Melchior (eds) Urodynamics N.Y.: Springer-Verlag pp. 1-13.

Brennen, C. and H. Winet (1977) "Fluid mechanics of propulsion by cilia and flagella" Ann. Rev. Fluid Mech. 9: 339-398.

Bueno, L., J. Fioramonti and Y. Ruckebusch (1975) "Rate of flow of digesta and electrical activity of the small intesine in dogs and sheep" J. Physiol., Lond. 249: 69-85.

Cannon, W.B. (1911) The Mechanical Factors of Digestion N.Y.: Longmans Green and Co. pp. 131-133.

Caro, C.G., T.J. Pedley, R.C. Schroter and W.A. Seed (1978) The Mechanics of the Circulation N.Y.: Oxford U. Press.

Charm, S.E. and G.S. Kurland (1974) Blood Flow and Microcirculation N.Y.: John Wiley.

Christensen, J. (1981) "Motility of the colon" in L.R. Johnson (ed) Physiology of the Gastrointestinal Tract N.Y.: Raven Press pp. 445-471.

Davenport, H.W. (1977) Physiology of the Digestive Tract Chicago: Year Book Medical Publishers pp. 58-83.

Fung, Y.C. (1981) Biomechanics N.Y.: Springer-Verlag.

Gerrard, J.H. (1982) "Numerical analysis and linear theory of pulsatile flow in cylindrical deformable tubes: The testing of a numerical model for blood flow calculation" Med. Biol. Eng. Comput. 20: 49-57.

Gray, J. and G.J. Hancock (1955) "The propulsion of sea-urchin spermatozoa" J. exp. Biol. 32: 802-814.

Grivel, M.-L. and Y. Ruckebusch (1972) "The propagation of segmental contractions along the small intestine" J. Physiol. Lond. 227: 611-625.

Guier, W.H. (1980) "A hemodynamic model for relating phasic pressure and flow in large arteries" IEEE Trans. Biom. Eng. BME 27: 479-482.

Henderson, R.D. (1980) The Esophagus Baltimore: Williams and Wilkins.

Hancock, G.J. (1953) "The self-propulsion of microscopic organisms through liquids" Proc. Roy. Soc. Lond. A 217: 96-121.

Hook, S.J. and E.S.E. Hafez (1968) A comparative anatomical study of the mammalian uterotubal junction" J. Morphol. 125: 159-184.

Keller, S.R., T.Y. Wu and C. Brennen (1975) "A tranction-layer model for ciliary propulsion" in T.Y. Wu, C.J. Brennen and C.J. Brokaw (eds) Swimming and Flying in Nature V.1 N.Y.: Plenum Press pp.253-271.

Kerlin, P., A. Zinsmeister and S. Phillips (1982) "Relationship of motility to flow of contents in the human small intestine" Gastroent. 82: 701-706.

Klauser, S.C., T.J. Blair, W.F. Bulawa, G.M. Jeppson, R.L. Jensen and P.D. Clayton (1982) "Quantitative analysis of segmental wall motion throughout systole and diastole in the normal human left ventricle" Circulation 65: 580-590.

Lapides, J. and A.C. Diokno (1976) "Urine transport, storage and micturation" in J. Lapides (ed) Fundamentals of Urology Philadelphia: W.B. Saunders pp. 190-200.

Lassen, N.A. and W. Perl (1979) Tracer Kinetic Methods in Medical Physiology N.Y.: Raven Press.

Lee, C.S.F. and L. Talbot (1979) "A fluid-mechanical study of the closure of heart valves" J. Fluid Mech. 91: 41-63.

Lipowski, H.H. and B.W. Zweifach (1977) "Methods for the simultaneous measurement of pressure differentials and flow in single unbranched vessels of the microcirculation for rheological studies" Microvas. Res. 14: 345-361.

Liron, N. (1978) "Fluid transport by cilia between parallel plates" J. Fluid Mech. 86: 705-726.

Liron, N. and S. Mochon (1976) "Stokes flow for a stokeslet between two parallel flat plates" J. Eng. Math. 10: 287-303.

Liron, N. and R. Shahar (1978) "Stokes flow due to a stokeslet in a pipe" J. Fluid Mech. 86: 727-744.

Macagno, E.O. and J. Christensen (1980) "Fluid mechanics of the duodenum" Ann. Rev. Fluid Mech. 12: 139-158.

Macagno, E.O. and J. Christensen (1981) "Fluid mechanics of gastrointestinal flow" in L.R. Johnson (ed) Physiology of Gastrointestinal Tract N.Y.: Raven Press pp. 335-358.

Macagno, E.O. and T.K. Hung (1967) "Computational and experimental study of a captive annular eddy" J. Fluid Mech. 28: 43-64.

Macagno, E., J. Melville and J. Christensen (1975) "A model for longitudinal motility of the small intestine" Biorheol. 12: 369-376.

McCall, A.L., W.P. Potsie, C.K. Shih, M. Litt and M.A. Khan (1978) "Physicochemical properties of human middle ear effusions (mucus) and their relation to ciliary transport" Laryngoscope 88: 729-738.

Melchior, H. and W. Lutzeyer (1973) "Functional parameters of ureteral peristalsis" in W. Lutzeyer and H. Melchior (eds) Urodynamics N.Y.: Springer-Verlag pp. 71-79.

Misiewicz, J.J. (1980) "Motility" in W. Sircus and A.N. Smith (eds) Scientific Foundations of Gastroenterology Philadelphia: W.B. Saunders pp. 483-491.

Morris, J.L. (1981) "Structure and function of ciliated peritoneal funnels in the toad kidney (Bufo marinus)" Cell Tiss. Res. 217: 599-610.

Nelson, D.J. and E.M. Wright (1974) "The distribution, activity and function of the cilia in the frog brain" J. Physiol. Lond. 243: 63-78.

Patel, P.D., B.F. Picologlou and P.S. Lykoudis (1973) "Biorheological aspects of colonic activity. Part II. Experimental investigation of the rheological behavior of human faeces" Biorheol. 10: 441-445.

Pescatori, M., B. Marsicano, R. Mancinelli, S. Salinari and A. Bertuzzi (1980) "Control of peristalsis in the isolated rabbit colon" in J. Christensen (ed) Gastrointestinal Motility N.Y.: Raven Press pp. 479-486.

Picologlou, B.F., P.D. Patel and P.S. Lykoudis (1973) "Biorheological aspects of colonic activity. Part I. Theoretical considerations" Biorheol. 10: 431-440.

Pollack, and Wood (1949) "Venous pressure in the saphenous vein at the ankle in man during exercise and changes in posture" J. appl. Physiol. 1: 656-

Roberts, A.M. (1970) "Motion of spermatozoa in fluid streams" Nature 228: 375-376.

Ross, S.M. and S. Corrsin (1974) "Results of an analytical model of mucociliary pumping" J. Appl. Physiol. 37: 333-340.

Rouse, H. and S. Ince (1957) History of Hydraulics N.Y.: Dover Publ.

Schultz, D.L., D.S. Tunstall-Pedoe, G. de J. Lee, A.J. Gunning and B.J. Bellhouse (1969) "Velocity distibution and transition in the arterial system" in G.E.W. Wolstenholme and J. Knight (eds) Circulatory and Respiratory Mass Transport London: J. and A. Churchill pp. 172-202.

Shapiro, A.H. (1977) "Steady flow in collapsible tubes" Trans. ASME J. Biomech. Eng. 99: 126-147.

Shapiro, A.H. and M.Y. Jaffrin (1971) "Reflux in peristaltic pumping: Is it determined by Eulerian or Lagrangian mean velocity?" J. appl. Mech. 38: 1060-1062.

Shen, M.C. (1976) "Asymptotic theory for peristaltic transport in a tube of arbitrary cross section" Physics of Fluids 19: 213-218.

Shen, M.C. and S.M. Shih (1978) "Comments on 'Asymptotic theory for peristaltic transport in a tube of arbitrary cross section'" Phys. Fluids 21: 1663-1664.

Shen, M.C., S.M. Shim and A.M. Wu (1980) "Asymptotic method for peristaltic transport" Bull. Math. Biol. 42: 305-326.

Singerman, R.B. (1974) Fluid Mechancs of the Duodenum Ph.D. Thesis University of Iowa.

Singerman, R.B., E.O. Macagno, J.R. Glover and J. Christensen (1975) "Stochastic model of contractions at a point in the duodenum" Am. J. Physiol. 229: 613-617.

Skalak, R. and S. Chien (1981) "Capillary flow: History, experiments and theory" Biorheol. 18: 307-330.

Sokeland, J., P. May, K. Haubensak and K. Schulte (1973) "The potential value of urodynamic measurements in clinical practice" in W. Lutzeyer and H. Melchior (eds) Urodynamics N.Y.: Springer-Verlag pp. 26-29.

Swabb, E.A., R.A. Hynes and M. Donowitz (1982a) "Elevated intraluminal pressure alters rabbit small intestinal transport in vivo" Am. J. Physiol. 242: G58-G64.

Swabb, E.A., R.A. Hynes, W.G. Marnane, J.S. McNeil, R.A. Decker, Y.h. Tai and M. Donowitz (1982b) "Intestinal filtration-secretion due to increased intraluminal pressure in rabbits" Am. J. Physiol. 242: G65-G75.

Talbot, L. and S.A. Berger (1974) "Fluid mechanical aspects of human circulation" Am. Sci. 62: 671-682.

Talo, A. (1981) "In-vitro spontaneous electrical activity of rat efferent ductules" J. Reprod. Fert. 63: 17-20.

Vann, P.G. and J.R. Blake (1982) "Mechanics of ovum transport in the oviduct" Cell Motil. 1(Suppl.): 53-57.

Vantrappen, G.R. and J. Hellemans (1980) "Motility" in W. Sircus and A.N. Smith (eds) Scientific Foundations of Gastroenterology Philadelphia: W.B. Saunders pp. 227-253.

Verdugo, P., W.I. Lee, S.A. Halbert, R.J. Blandau and P.Y. Tam (1980) "A stochastic model for oviductal egg transport" Biophys. J. 29: 257-270.

Walburn, F.J. and P.D. Stein (1980) "Flow characteristics in symmetrically branched tubes simulating the human aortic bifrication" Trans. ASME J. Biomech. Eng. 102: 340-342.

Walburn, F.J. and P.D. Stein (1981) "Effect of vessel tapering on the transition to turbulent flow: Implications in the cardiovascular system" Trans. ASME J. Biomech. Eng. 103: 116-120.

Ward-Smith, A.J. (1980) Internal Fluid Flow Oxford: Clarendon Press.

Weems, W.A. (1981) "The intestine as a fluid propelling system" Ann. Rev. Physiol. 43: 9-19.

Weems, W.A. and G.E. Seygal (1980) "Intestinal propulsion: Studies employing a method for its quantitative evaluation" in J. Christensen (ed) Gastrointestinal Motility N.Y.: Raven Press pp. 331-338.

Weems, W.A. and G.E. Seygal (1981) "Fluid propulsion by cat intestinal segments under conditions requiring hydrostatic work" Am. J. Physiol. 240: G147-G156.

Weisbrodt, N.M. (1981) "Motility of the small intestine" in L.R. Johnson (ed) Physiology of the Gastrointestinal Tract N.Y.: Raven Press pp. 411-443.

Winet, H. (1976) "Ciliary propulsion of objects in tubes: Wall drag on swimming Tetrahymena (Ciliata) in the presence of mucin and other long-chain polymers" J. exp. Biol. 64: 283-302.

Winet, H. (1980a) "On the mechanism for flow in the efferent ducts" J. Androl. 1: 304-311.

Winet, H. (1980b) "Reflux in ciliated channels and its implications for propulsion in the oviduct" Fed. Proc. 39: 825.

Winet, H. and J.R. Blake (1980) "On the mechanics of mucociliary flows. I. Observations of a channel model" Biorheol. 17: 135-150.

Winet, H., G.T. Yates, T.Y. Wu and J. Head (1982) "On the mechanics of mucociliary flows. II. A fluorescent tracer method for obtaining flow velocity profiles in mucus" Cell Motil. 1(Suppl.): 29-34.

Yang, S.S., L.G. Bentivoglio, V. Maranhao and H. Goldberg (1978) From Cardiac Catheterization Data to Hemodynamic Parameters

Philadelphia: F.A. Davis.
Yates, G.T., T.Y. Wu, R.E. Johnson, A.T.W. Cheung and C.L. Frand (1980) "A theoretical and experimental study on tracheal muco-ciliary transport" Biorheol. 17: 151-162.
Yin, F. and Y.C. Fung (1969) "Peristaltic waves in circular cylindrical tubes" A.S.M.E. J. Appl. Mech. 36: 579-587.

HW/jvs

SECURITY CLASSIFICATION OF THIS PAGE (When Data Entered)

REPORT DOCUMENTATION PAGE		READ INSTRUCTIONS BEFORE COMPLETING FORM
1. REPORT NUMBER #2456	2. GOVT ACCESSION NO. AD-A125284	3. RECIPIENT'S CATALOG NUMBER
4. TITLE (and Subtitle) On the Quantitative Analysis of Liquid Flow in Physiological Tubes		5. TYPE OF REPORT & PERIOD COVERED Summary Report - no specific reporting period 6. PERFORMING ORG. REPORT NUMBER
7. AUTHOR(s) H. Winet		8. CONTRACT OR GRANT NUMBER(s) HD-51442 DAAG29-80-C-0041
9. PERFORMING ORGANIZATION NAME AND ADDRESS Mathematics Research Center, University of Wisconsin 610 Walnut Street Madison, Wisconsin 53706		10. PROGRAM ELEMENT, PROJECT, TASK AREA & WORK UNIT NUMBERS Work Unit Number 2 - Physical Mathematics
11. CONTROLLING OFFICE NAME AND ADDRESS See Item 18 below		12. REPORT DATE December 1982 13. NUMBER OF PAGES 82
14. MONITORING AGENCY NAME & ADDRESS(if different from Controlling Office)		15. SECURITY CLASS. (of this report) UNCLASSIFIED 15a. DECLASSIFICATION/DOWNGRADING SCHEDULE

16. DISTRIBUTION STATEMENT (of this Report)

Approved for public release; distribution unlimited.

17. DISTRIBUTION STATEMENT (of the abstract entered in Block 20, if different from Report)

18. SUPPLEMENTARY NOTES

U. S. Army Research Office
P. O. Box 12211
Research Triangle Park
North Carolina 27709

National Institutes of Health
Bethesda, Maryland 20205

19. KEY WORDS (Continue on reverse side if necessary and identify by block number)

Flow in physiological tubes, pulsatile flow, ciliary flows, peristaltic/ segmented flows, combination pumps.

20. ABSTRACT (Continue on reverse side if necessary and identify by block number)

We review three benchmark quantitative models for flow generation by physiological tube pumps. In each case significant differences between model predictions and tube behavior was emphasized. In order to close these gaps both modeler and Physiologist (often the same investigator) need to find paths which can grow to bridges. The modeler must develop more exact solutions to provide Physiologists with plug-in equations which will accept measurements. The Physiologist must make the kind of measurements which can be reasonably tested by a meaningful model. The measurements which have been featured in this review

DD FORM 1 JAN 73 1473 EDITION OF 1 NOV 65 IS OBSOLETE

UNCLASSIFIED

SECURITY CLASSIFICATION OF THIS PAGE (When Data Entered)

ABSTRACT (continued)

are pressure, viscosity and geometry--or where geometry varies with time, kinematic data. A number of diagnostic marker formulas have been presented as stepping stones to modeling. These include R_e, β, slenderness etc. which translate physiological data into indicators for modeling directions.